Elevated TGFβ signaling contributes to ocular anterior segment dysgenesis in *Col4a1* mutant mice

Mao Mao [a], Cassandre Labelle-Dumais [a], Sara F. Tufa [b], Douglas R. Keene [b] and Douglas B. Gould [a,c,d,e,f]

***a* - Department of Ophthalmology,** *University of California, San Francisco, San Francisco, CA 94143, United States*
***b* - Shriners Children's, Micro-Imaging Center,** *Portland, Oregon 97239, United States*
***c* - Department of Anatomy,** *University of California, San Francisco, San Francisco, CA 94143, United States*
***d* - Institute for Human Genetics,** *University of California, San Francisco, San Francisco, CA 94143, United States*
***e* - Cardiovascular Research Institute,** *University of California, San Francisco, San Francisco, CA 94143, United States*
***f* - Bakar Aging Research Institute,** *University of California, San Francisco, San Francisco, CA 94143, United States*

Corresponding author at: *Department of Ophthalmology, University of California, San Francisco, San Francisco, CA 94143, United States. Douglas.Gould@ucsf.edu.*
https://doi.org/10.1016/j.matbio.2022.05.001

Abstract

Ocular anterior segment dysgenesis (ASD) refers to a collection of developmental disorders affecting the anterior structures of the eye. Although a number of genes have been implicated in the etiology of ASD, the underlying pathogenetic mechanisms remain unclear. Mutations in genes encoding collagen type IV alpha 1 (COL4A1) and alpha 2 (COL4A2) cause Gould syndrome, a multi-system disorder that often includes ocular manifestations such as ASD and glaucoma. COL4A1 and COL4A2 are abundant basement membrane proteins that provide structural support to tissues and modulate signaling through interactions with other extracellular matrix proteins, growth factors, and cell surface receptors. In this study, we used a combination of histological, molecular, genetic and pharmacological approaches to demonstrate that altered TGFβ signaling contributes to ASD in mouse models of Gould syndrome. We show that TGFβ signaling was elevated in anterior segments from *Col4a1* mutant mice and that genetically reducing TGFβ signaling partially prevented ASD. Notably, we identified distinct roles for TGFβ1 and TGFβ2 in ocular defects observed in *Col4a1* mutant mice. Importantly, we show that pharmacologically promoting type IV collagen secretion or reducing TGFβ signaling ameliorated ocular pathology in *Col4a1* mutant mice. Overall, our findings demonstrate that altered TGFβ signaling contributes to COL4A1-related ocular dysgenesis and implicate this pathway as a potential therapeutic target for the treatment of Gould syndrome.

Introduction

Ocular anterior segment dysgenesis (ASD) refers to a spectrum of clinically and genetically heterogeneous diseases affecting the development of ocular tissues anterior to the vitreous surface: cornea, iris, lens, ciliary body, and drainage structures responsible for aqueous humor efflux. ASD clinical manifestations include corneal opacity, posterior embryotoxon (anteriorly displaced Schwalbe's line), iris hypoplasia, abnormal pupil formation, iridocorneal adhesions, corneolenticular adhesions, and cataract. Notably, individuals with ASD are at increased risk of experiencing visual impairment and developing glaucoma as structural ocular malformations can obstruct the light path, and impair aqueous humor outflow and intraocular pressure homeostasis [1–4]. ASD etiology is complex and multiple genes and developmental processes have been implicated. Development of anterior ocular structures relies on a series of highly orchestrated interactions between the surface ectoderm, neural

ectoderm, and the periocular mesenchyme. Mutations in several genes have been reported in ASD, many of which encode transcription factors. Among them, *FOXC1* and *PITX2* are the most studied ASD genes and mutations in *FOXC1* and *PITX2* account for approximately 40% of all ASD cases [5]. *FOXC1* and *PITX2* are both expressed in the periocular mesenchyme, which gives rise to the majority of anterior segment tissues, and play important roles in mesenchymal cell specification and differentiation [2]. However, the mechanisms by which FOXC1 and PITX2 regulate these processes remain elusive. The widespread adoption of next-generation sequencing has broadened the genetic landscape for ASD as an increasing number of genes are being discovered; however, the genetic causes in many ASD cases remain to be identified and the underlying pathogenic mechanisms are poorly understood [6].

Recent genetic studies have highlighted the importance of the extracellular matrix (ECM) in ocular development and ASD [6,7]. Notably, mutations in genes encoding the major basement membrane (BM) components collagen type IV alpha 1 (COL4A1) and alpha 2 (COL4A2) cause Gould syndrome, which is characterized by a broad range of cerebrovascular, ocular, muscular, renal, or cardiac manifestations [8–10]. Gould syndrome has a highly variable clinical presentation in which disease severity and penetrance differ even among individuals within the same family [11–13]. Most of the mutations identified so far are dominant missense mutations; however, recessive, nonsense, splicing, and frameshift mutations, intragenic insertions and deletions, 3′-UTR mutations affecting miRNA binding sites, as well as gene duplications, have also been described [9,14–23]. Hundreds of mutations have now been reported in the literature and ASD-related manifestations occur in approximately 30% of the cases [9,24]. Despite increasing awareness of Gould syndrome, the pathogenic processes involved remain to be defined. We and others have demonstrated previously that *Col4a1* and *Col4a2* mutant mice recapitulate the pathophysiological hallmarks of Gould syndrome, including ocular dysgenesis and glaucoma-relevant phenotypes, and represent valuable pre-clinical models to study the underlying disease mechanisms [25–33]. Notably, using an allelic series of *Col4a1* and *Col4a2* mutations and studying the effect of different genetic backgrounds in mice, we have shown that allelic heterogeneity, genetic context, and tissue-specific mechanistic heterogeneity all contribute to the variable expressivity of *Col4a1 and Col4a2* mutations [10,30,32–35]. A better understanding of the molecular mechanisms by which *Col4a1* mutations lead to ASD will provide insights into the pathogenic processes underlying ASD and glaucoma and could have important implications for patient stratification and the development of personalized medicine for individuals with Gould syndrome.

COL4A1 and COL4A2 proteins represent fundamental BM components of every organ in the body, including the eye [36]. COL4A1 and COL4A2 contain three major domains: a short amino-terminal 7S domain, a long collagenous triple-helical domain, and a globular non-collagenous domain at the carboxy-terminus. One COL4A2 and two COL4A1 proteins assemble into heterotrimers [α1α1α2(IV)] in the endoplasmic reticulum (ER) before being secreted into the extracellular space where they form an intricate network and interact with other ECM components, growth factors, and cell surface receptors [37,38]. Most *Col4a1* and *Col4a2* mutations impair protein folding during heterotrimer formation, resulting in intracellular accumulation and impaired secretion of collagen α1α1α2(IV) heterotrimers, both of which could constitute primary pathogenic events [25,33]. For instance, accumulation of misfolded proteins in the ER can trigger chronic ER stress and cytotoxicity which could act as a cell-autonomous or 'proximal' insult [39]. In contrast, the concomitant extracellular deficiency, and in some cases the presence of mutant proteins in the BM, can impair BM integrity and/or functions of the collagen α1α1α2(IV) network and represent distinct classes of extracellular or 'distal' insults. However, the various biological functions of type IV collagens are not fully characterized and the downstream consequences of having reduced collagen α1α1α2(IV) levels or the presence of mutant collagen α1α1α2(IV) in the BM are largely unknown. This represents an important knowledge gap and a major obstacle to developing targeted mechanism-based interventions for individuals with Gould syndrome.

Independent lines of evidence suggest that type IV collagens can regulate transforming growth factor beta (TGFβ) superfamily signaling pathways, raising the possibility that perturbations of TGFβ superfamily signaling could represent a distal insult in the context of *Col4a1* and *Col4a2* mutations. Notably, type IV collagens can directly bind to TGFβ superfamily ligands such as TGFβ1 and BMP4 *in vitro* [40–42] and *Drosophila* orthologs of type IV collagen control BMP signaling during embryogenesis, organogenesis, and maintenance of germline stem cells [41,43]. Furthermore, members of the TGFβ superfamily play important roles in anterior segment development by promoting survival, migration, and differentiation of the periocular mesenchyme [44–46]. Mice that lack TGFβ2 [45] or the TGFβ type 2 receptor (TGFBR2) in neural crest-derived periocular mesenchyme [44] have thin corneal stroma, and fail to form corneal endothelium, trabecular meshwork, and anterior chambers. While mice deficient for TGFβ1 or TGFβ3 have no apparent ocular phenotypes [47–49], overexpression of TGFβ1 in the lens lead

to abnormally thick corneal stroma [46]. Similarly, mice deficient for other members of the TGFβ superfamily [50], their antagonists [51,52], and downstream signaling mediators [53,54] develop severe ASD and mutations in *BMP4, BMP7* and *CHRDL1* are reported in individuals with ASD [55,56]. Based on these findings, we hypothesized that collagen α1α1α2(IV) heterotrimers act as extracellular regulators of TGFβ and/or BMP signaling in ocular development and disease. In this study, we used a combination of histological, molecular, genetic, and pharmacological approaches to show that elevated canonical TGFβ signaling contributes to ASD in *Col4a1* mutant mice. In addition, we show that genetically or pharmacologically reducing TGFβ signaling can partially prevent ocular defects in *Col4a1* mutant mice, suggesting that the TGFβ signaling pathway represents a potential therapeutic target for Gould syndrome.

Results

Col4a1$^{+/\Delta ex41}$ mice have developmental corneal defects

We previously described a *Col4a1* splice site mutation that results in skipping of exon 41 (*Col4a1*$^{\Delta ex41}$) [25,30,31] and showed that *Col4a1*$^{+/\Delta ex41}$ mice have severe ASD characterized by open pupil, pigment dispersion, iridocorneal dysgenesis, enlarged anterior chamber, tortuous iris vasculature, and cataracts [30]. Here, we show that *Col4a1*$^{+/\Delta ex41}$ mice also have developmental corneal defects resulting in abnormally thin corneas (Fig. 1). At embryonic day 18.5 (E18.5), the corneal epithelium and endothelium are both one cell layer thick and the majority of the corneal thickness is contributed by the corneal stroma [52]. Histological analyses revealed that corneal stromal thickness was significantly reduced in *Col4a1*$^{+/\Delta ex41}$ compared to *Col4a1*$^{+/+}$ mice (Fig. 1A). By 1.6–2.0 months of age, while the majority of *Col4a1*$^{+/\Delta ex41}$ corneas are transparent, optical coherence tomography (OCT) imaging showed that the central corneal thickness (CCT) remained significantly reduced in *Col4a1*$^{+/\Delta ex41}$ mice compared to *Col4a1*$^{+/+}$ littermates (Fig. 1B). Consistent with our previous findings [30], OCT also revealed a significant increase in anterior chamber depth which contributed to a small but significant increase in ocular axial length (Fig. S1). Reduced lens diameter and retinal thickness, and increased vitreous chamber depth were also observed in *Col4a1*$^{+/\Delta ex41}$ eyes (Fig. S1). Together, these findings show that *Col4a1*$^{+/\Delta ex41}$ mice have reduced corneal thickness from development through adulthood and demonstrate the presence of defects in other ocular structures.

The corneal stroma is mainly composed of ECM secreted by sparsely distributed keratocytes [51]. To investigate the cause of reduced CCT, we first evaluated the number of keratocytes in *Col4a1*$^{+/\Delta ex41}$ mice. To this end, we used DAPI staining to quantify the total number of corneal stromal nuclei in E18.5 mice (Fig. 1C). No difference in the total number of nuclei was observed between *Col4a1*$^{+/+}$ and *Col4a1*$^{+/\Delta ex41}$ mice; however, the density was higher in the thinner corneas from *Col4a1*$^{+/\Delta ex41}$ mice. Next, we performed qPCR analyses on anterior segments from postnatal day 7 (P7) mice to test whether alterations in the expression of ECM components contributed to changes in corneal thickness (Fig. 1D). We found that expression levels for major constituents of mammalian corneal stroma (type I and type V collagens) [51] and matrix molecules implicated in corneal thinning [57–59] were similar between *Col4a1*$^{+/+}$ and *Col4a1*$^{+/\Delta ex41}$ mice. However, the expression of *Col15a1* and *Col18a1,* which encode BM-associated collagens, was reduced in *Col4a1*$^{+/\Delta ex41}$ anterior segments. A thin BM called Descemet's membrane is deposited by the corneal endothelium and separates the endothelium from the stroma. Because *Col15a1* and *Col18a1* mRNA levels were reduced, we evaluated the expression of corneal endothelial markers and found that *Cdh2* and *Gja1* mRNA levels were also reduced in anterior segments from P7 *Col4a1*$^{+/\Delta ex41}$ mice, while *Ocln* mRNA levels were increased (Fig. 1E). Consistent with this observation, CDH2 protein levels were also decreased in anterior segments from P7 *Col4a1*$^{+/\Delta ex41}$ mice (Fig. 1F). Moreover, immunolabeling revealed a reduction in CDH2 levels in the corneal endothelium in two out of four P7 corneal whole mounts tested (Fig. 1G).

We next performed transmission electron microscopy (TEM) to investigate ultrastructural corneal morphology in neonatal and adult mice. TEM analyses revealed regular stromal organization of collagen fibrils in lamellar arrangements in *Col4a1*$^{+/+}$ and *Col4a1*$^{+/\Delta ex41}$ mice at both ages examined (Fig. S2). However, in the posterior stroma of P0 mice we observed regions of higher cellular density and densely packed collagen fibrils in *Col4a1*$^{+/\Delta ex41}$ compared to *Col4a1*$^{+/+}$ mice (Fig. S2A). At 2.5 months of age, the collagen lamellae appeared denser and thinner in two out of three corneas from *Col4a1*$^{+/\Delta ex41}$ mice (Fig. S2B). Further, granular material was observed posterior to the corneal epithelium in 2 out of 3 *Col4a1*$^{+/\Delta ex41}$ corneas, one of which also had disrupted epithelial basement membrane (Fig. S2C). In addition, while the morphology of the corneal endothelium was unremarkable, Descemet's membrane was thinner in *Col4a1*$^{+/\Delta ex41}$ mice at 2.5 months of age (Fig. S2C,D). Upon higher magnification, we observed normal fibril structures in *Col4a1*$^{+/+}$ and *Col4a1*$^{+/\Delta ex41}$ stroma at both ages examined (Fig. S3A,B). However, the

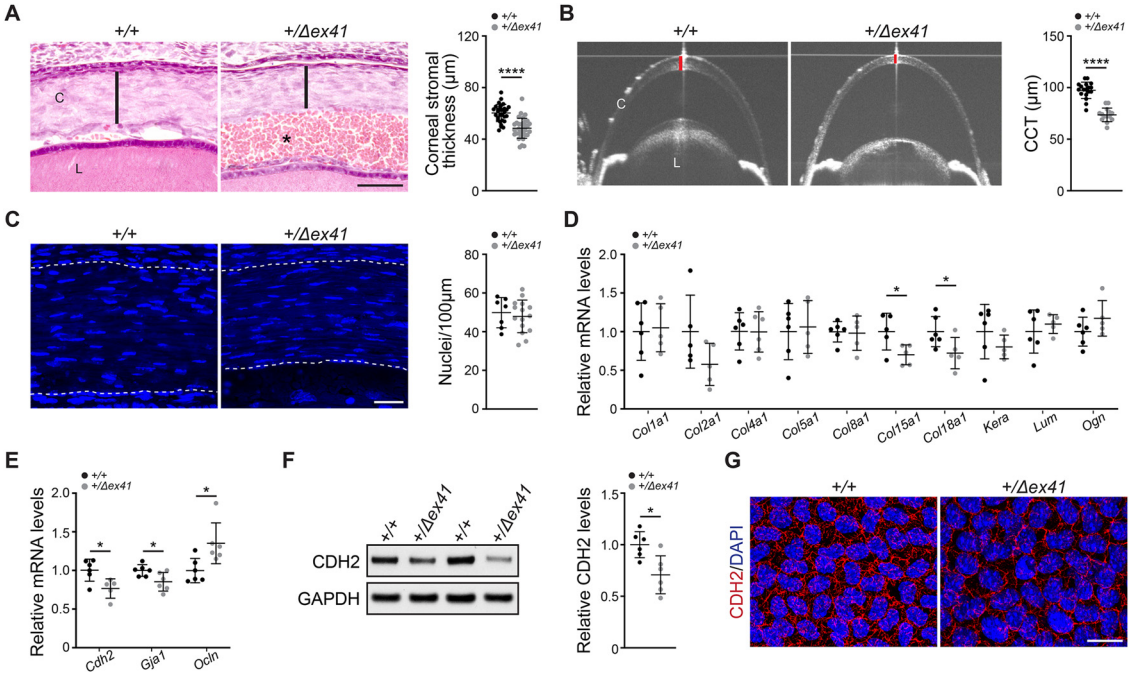

Fig. 1. *Col4a1*$^{+/\Delta ex41}$ mice have developmental corneal defects. (**A**) Representative images (left) and quantification (right) of E18.5 H&E stained ocular sections showing reduced corneal stromal thickness (black bars) in *Col4a1*$^{+/\Delta ex41}$ mice. Asterisk indicates anterior hyphema. $n = 31$ *Col4a1*$^{+/+}$and 33 *Col4a1*$^{+/\Delta ex41}$ corneas. Scale bar = 50 μm. (**B**) Representative OCT images (left) and quantification (right) of anterior segments showing reduced CCT (red bars) in *Col4a1*$^{+/\Delta ex41}$ compared to *Col4a1*$^{+/+}$ mice at 1.6−2.0 months. $n = 18$ *Col4a1*$^{+/+}$and 14 *Col4a1*$^{+/\Delta ex41}$ eyes. (**C**) Representative images (left) and quantification (right) of E18.5 corneas stained with DAPI (blue) showing that the number of corneal stromal nuclei was indistinguishable between *Col4a1*$^{+/+}$and *Col4a1*$^{+/\Delta ex41}$ mice, suggesting that corneal thinning in *Col4a1*$^{+/\Delta ex41}$ mice is not caused by a reduction in the number of keratocytes. Dashed lines indicate the stromal boundaries. $n = 7$ *Col4a1*$^{+/+}$and 15 *Col4a1*$^{+/\Delta ex41}$ corneas. Scale bar = 20 μm. (**D** and **E**) qPCR analyses showing the relative mRNA levels of genes encoding major corneal matrix molecules (D) and corneal endothelial markers (E) in P7 anterior segments. $n = 5–6$ per genotype. Data shown as fold expression relative to wildtype. (**F**) Representative Western blot images (left) and quantification (right) showing reduced CDH2 protein levels in P7 anterior segments from *Col4a1*$^{+/\Delta ex41}$ mice. $n = 6$ per genotype. Data shown as fold expression relative to wildtype. (**G**) Representative images of P7 corneal flat mounts immunolabeled for CDH2. Two out of four *Col4a1*$^{+/\Delta ex41}$ corneas examined showed reduced CDH2 labeling intensity compared to their *Col4a1*$^{+/+}$counterparts. Scale bar = 20 μm. $n = 4$ per group. C, cornea; L, lens. Data are presented as mean ± SD. *$p < 0.05$; ****$p < 0.0001$, Student's t-test.

distribution of fibril diameters showed a significant shift toward smaller fibrils in *Col4a1*$^{+/\Delta ex41}$ mice and the mean fibril density tended to be higher in *Col4a1*$^{+/\Delta ex41}$ corneas (Fig. S3C−F), suggesting that collagen fibrils are smaller and more densely packed. Taken together, our results indicate that *Col4a1*$^{+/\Delta ex41}$ mice show aberrant corneal development characterized by reduced corneal thickness, thinner and denser collagen lamella composed of smaller and more densely packed fibrils, altered expression of corneal endothelial markers, and thinner Descemet's membrane.

Evaluating the potential contribution of FOXC1 and PITX2 transcriptional networks to ASD in *Col4a1* mutant mice

The majority of ocular anterior segment structures, including the corneal stroma and endothelium, are derived from periocular mesenchyme that migrates between the corneal epithelium and lens during development [60]. FOXC1 and PITX2 are transcription factors that are critical for periocular mesenchyme differentiation and are the two most frequently mutated genes in human ASD [2]. FOXC1 and PITX2 functionally interact during ocular development and are both sensitive to gene dosage with either decreased or increased expression having pathological consequences [2]. To test whether ASD in *Col4a1* mutant mice mechanistically converges on the FOXC1 and/or PITX2 transcriptional networks, we assessed the expression levels of *Foxc1, Pitx2*, their downstream targets, and binding partners in eyes from *Col4a1*$^{+/\Delta ex41}$ and *Col4a1*$^{+/+}$ littermates at E14.5, when the expression of these genes is the highest (Fig. S4). qPCR analyses revealed a small but significant reduction in *Foxc1* expression and a trend toward decreased

expression for the FOXC1 target gene *Tjp1* in *Col4a1*$^{+/\Delta ex41}$ eyes (Fig. S4A). Although *Pitx2* expression was unchanged, the mRNA levels for the PITX2 target gene *Slc13a3* [61] and the genes coding two PITX2 interacting proteins, EFEMP2 [62] and PAWR [63], were slightly but significantly reduced in *Col4a1*$^{+/\Delta ex41}$ eyes (Fig. S4B). To further explore potential contributions of the FOXC1 and PITX2 regulatory networks we attempted to validate these observations using a second *Col4a1* mutant mouse strain (*Col4a1*$^{+/G1344D}$). This strain carries a missense mutation that may represent a more accurate model of mutations reported in humans but has milder ASD than *Col4a1*$^{+/\Delta ex41}$ mice [33]. In contrast to what we observed in *Col4a1*$^{+/\Delta ex41}$ mice, none of those genes showed altered expression in *Col4a1*$^{+/G1344D}$ eyes (Fig. S4C,D). Though intriguing, our results do not settle whether abnormal regulation of the FOXC1 and PITX2 transcriptional networks contribute to ASD in *Col4a1* mutant mice.

TGFβ signaling is elevated in anterior segments of *Col4a1*$^{+/\Delta ex41}$ mice

Mutations in genes encoding various members of the TGFβ superfamily and their signaling mediators cause ASD in animal models and humans, and type IV collagens directly bind to TGFβ superfamily ligands *in vitro* and regulate their signaling in *Drosophila* [40–46]. Based on these observations, we hypothesized that aberrant TGFβ signaling could contribute to ASD in *Col4a1* mutant mice. To test this possibility, we first evaluated TGFβ signaling activity during anterior segment development in *Col4a1*$^{+/\Delta ex41}$ mice (Fig. 2). qPCR analyses revealed that the expression of the TGFβ target genes *Ccn2, Cdkn1a* and *Serpine1* was significantly increased in anterior segments from P7 *Col4a1*$^{+/\Delta ex41}$ mice compared to their *Col4a1*$^{+/+}$ littermates (Fig. 2A). Canonical TGFβ signaling is mediated by SMAD2/3 proteins, which are activated by phosphorylation before translocating to the nucleus to regulate gene expression (Fig. S5). To assess canonical TGFβ signaling *in vivo*, we crossed *Col4a1*$^{+/\Delta ex41}$ mice to the SBE-Luc TGFβ signaling reporter line which expresses luciferase in response to SMAD2/3-mediated TGFβ signaling [64]. Luciferase activity was significantly increased in P7 anterior segments from *Col4a1*$^{+/\Delta ex41}$*;SBE-Luc* mice compared to control *Col4a1*$^{+/+}$*;SBE-Luc* littermates (Fig. 2B,C). Consistent with this finding, Western blot analyses revealed a significant increase in the ratio of phosphorylated to total SMAD2 (pSMAD2:SMAD2) in P7 *Col4a1*$^{+/\Delta ex41}$ anterior segments (Fig. 2D). We repeated this experiment using different antibodies to detect SMAD2, SMAD3, and pSMAD2/3. While there appeared to be a reduction in total SMAD levels, the Western blot analyses confirmed increased ratios of phosphorylated to total SMAD2 and SMAD3 in P7 *Col4a1*$^{+/\Delta ex41}$ anterior segments (Fig. 2E). Furthermore, immunolabeling revealed increased pSMAD2 nuclear labeling intensity in corneal stromal cells from P7 *Col4a1*$^{+/\Delta ex41}$ mice compared to *Col4a1*$^{+/+}$ littermates (Fig. 2F). Taken together, these data indicate that canonical TGFβ signaling is elevated in developing anterior segments from *Col4a1*$^{+/\Delta ex41}$ mice.

In addition to TGFβs, several BMP family members play critical roles in the development of the ocular anterior segment [3]. To test if BMP signaling was also altered in *Col4a1*$^{+/\Delta ex41}$ mice, we performed qPCR analyses for BMP target genes in P7 anterior segments but did not detect changes in their expression levels (Fig. S6A). Similarly, Western blot analyses did not detect differences in the ratio of phospho-SMAD1/5/9 to total SMAD1/5/9 between P7 anterior segments from *Col4a1*$^{+/\Delta ex41}$ and *Col4a1*$^{+/+}$ littermates (Fig. S6B). In addition to the well-established role of canonical SMAD-mediated signaling [65], non-canonical TGFβ/BMP signaling pathways have also been implicated in ocular development and disease [66–69]. To determine whether non-canonical TGFβ signaling may play a role in ASD in *Col4a1* mutants, we used Western blot analyses to test the signaling activity of the p38 MAPK and ERK pathways and detected no difference in the ratios of phosphorylated to total p38 and ERK1/2 kinases in anterior segments from *Col4a1*$^{+/+}$ and *Col4a1*$^{+/\Delta ex41}$ mice (Fig. S6C,D). These findings suggest that perturbations in BMP and MAP kinase signaling are unlikely to contribute to anterior segment defects in *Col4a1*$^{+/\Delta ex41}$ mice and support the notion that abnormal canonical TGFβ signaling could play a predominant role in ASD pathogenesis.

The *Col4a1*^{G1344D} missense mutation also causes developmental corneal defects and elevated TGFβ signaling

To investigate further the role of altered TGFβ signaling in COL4A1-related ocular pathology, we extended our analyses to the *Col4a1*^{G1344D} mutation (Figs. 3, S7 and S8). OCT revealed that *Col4a1*$^{+/G1344D}$ mice have ocular defects including reduced CCT (Fig. 3A), enlarged anterior chamber, smaller lens, enlarged vitreous chamber depth, and thinner retina (Fig. S7). Furthermore, molecular analyses confirmed aberrant corneal endothelial marker expression in P7 *Col4a1*$^{+/G1344D}$ anterior segments (Fig. 3B,C). To determine if canonical TGFβ signaling was also elevated in the *Col4a1*$^{+/G1344D}$ mice, we evaluated pSMAD2/3 levels in P7 anterior segments using Western blot analysis. In contrast to our observations in *Col4a1*$^{+/\Delta ex41}$ mice, the pSMAD2/3:SMAD2/3 ratio was not significantly increased in anterior segments from *Col4a1*$^{+/G1344D}$ mice compared to *Col4a1*$^{+/+}$ littermates (Fig. 3D). To re-evaluate our hypothesis, we used an independent,

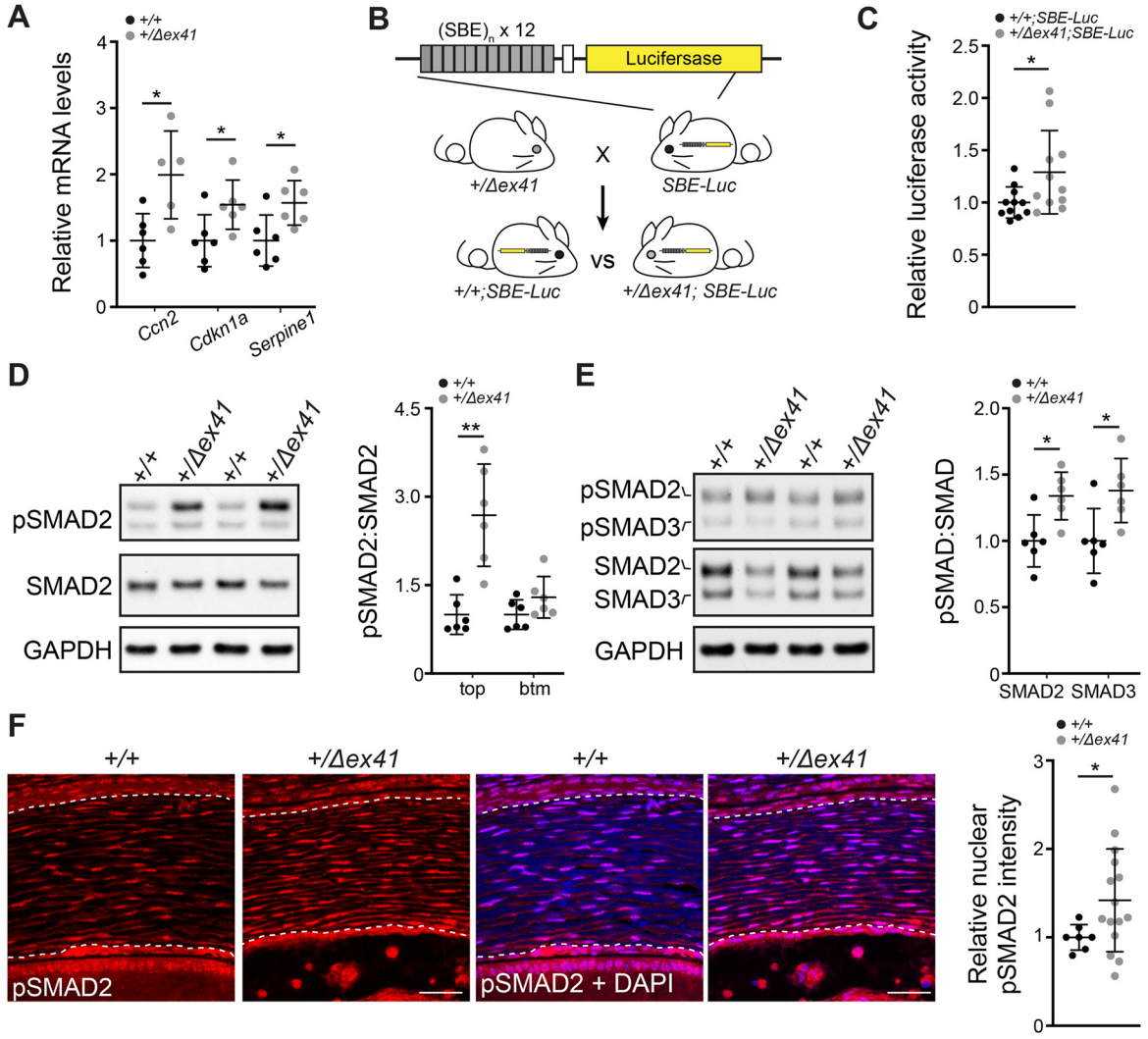

Fig. 2. TGFβ signaling is increased in developing anterior segments from *Col4a1*$^{+/\Delta ex41}$ *mice*. (**A**) qPCR analyses showing increased expression of the TGFβ target genes *Ccn2, Cdkn1a*, and *Serpine1* in anterior segments from P7 *Col4a1*$^{+/\Delta ex41}$ mice compared to *Col4a1*$^{+/+}$ littermates. *n* = 6 per genotype. (**B** and **C**) Schematic representation of the breeding strategy to generate *Col4a1*$^{+/+}$*;SBE-Luc* and *Col4a1*$^{+/\Delta ex41}$*;SBE-Luc* reporter mice (B) and quantification of luciferase activity using an *in vitro* luciferase assay (C) showing a significant increase in TGFβ signaling in P7 anterior segments from *Col4a1*$^{+/\Delta ex41}$*;SBE-Luc* mice compared to their *Col4a1*$^{+/+}$*;SBE-Luc* counterparts. *n* = 11 per genotype. Data shown as fold expression relative to *Col4a1*$^{+/+}$*;SBE-Luc* mice. (**D**) Representative Western blot images (left) and quantification (right) showing increased ratio of phosphorylated to total SMAD2 (pSMAD:SMAD2) protein levels in P7 anterior segments from *Col4a1*$^{+/\Delta ex41}$ mice compared to *Col4a1*$^{+/+}$ littermates. *n* = 6 per genotype. Because the pSMAD2 antibody recognized two bands, quantification was done separately for each band. (**E**) Representative Western blot images (left) and quantification (right) using antibodies recognizing both SMAD2 and SMAD3 showing increased pSMAD2:SMAD2 and pSMAD3:SMAD3 in P7 anterior segments from *Col4a1*$^{+/\Delta ex41}$ mice compared to *Col4a1*$^{+/+}$ littermates. *n* = 6 per genotype. Samples used in (D) and (E) were obtained from independent cohorts. (**F**) Representative images (left) of corneas immunolabeled for pSMAD2 (red) and counterstained with DAPI (blue), and quantification of corneal nuclear pSMAD2 labeling intensity (right) showing increased pSMAD2 levels in E18.5 *Col4a1*$^{+/\Delta ex41}$ mice compared to *Col4a1*$^{+/+}$ littermates. Scale bar = 20 μm. *n* = 7 *Col4a1*$^{+/+}$and 15 *Col4a1*$^{+/\Delta ex41}$ corneas. Data are presented as mean ± SD. **p* < 0.05; ***p* < 0.01, Student's t-test.

unbiased bulk RNA-seq approach to perform a comparative transcriptome analysis between anterior segments from *Col4a1*$^{+/+}$ and *Col4a1*$^{+/G1344D}$ eyes at P0. We chose this age because *Col4a1* mutant eyes appear grossly normal, with the exception of thin CCT and anterior hyphema [30], and sufficient amounts of RNA can be isolated by pooling four anterior segments per sample. Functional enrichment analysis of differentially expressed genes (DEGs) between *Col4a1*$^{+/+}$ and *Col4a1*$^{+/G1344D}$

anterior segments revealed multiple significantly enriched biological processes and molecular pathways including angiogenesis and cell adhesion (Fig. S8). Importantly, the WikiPathway "TGFbeta signaling pathway" (WP113) and the gene ontology (GO) term "Response to transforming growth factor beta (GO0071059)" are among the top enriched pathways or biological process terms identified using two different types of functional enrichment analysis methods and were predicted to be upregulated by both tools (Fig. 3E,F), supporting that TGFβ signaling is enhanced in eyes from *Col4a1*$^{+/G1344D}$ mice. To validate the RNA-seq results, we selected 13 DEGs that were previously reported to be induced by TGFβ activation from the enriched "Response to transforming growth factor beta (GO0071059)" category and tested them in independent biological replicates. Seven out of 13 genes tested by qPCR showed significantly elevated expression, and 2 additional genes showed trends towards significance (Fig. 3G), supporting the existence of elevated TGFβ signaling in P0 anterior segments from *Col4a1*$^{+/G1344D}$ mice. Collectively, our data demonstrate that TGFβ signaling is elevated in developing eyes from *Col4a1* mutant mice and raises the possibility that it might contribute to ASD.

Differential contributions of TGFβ1 and TGFβ2 to ocular defects observed in *Col4a1*$^{+/G1344D}$ mice

To test whether elevated TGFβ signaling contributes to ASD in *Col4a1* mutant mice we sought to experimentally reduce TGFβ signaling *in vivo* by genetically inactivating TGFβ ligands (Figs. 4, S5, S9 and S10). Expression of all three TGFβ ligand isoforms has been reported in the developing eye and their receptors are ubiquitously expressed in the periocular mesenchyme [44,70,71]. TGFβ2 is the predominant ligand isoform in the developing mouse eye and inactivation of TGFβ2, but not TGFβ1 or TGFβ3, lead to ocular malformations [44,47–49]. In contrast, TGFβ1 shows little expression in ocular structures [44,70]; however, it is abundantly present in the circulation [72] and the vasculature [70,73]. TGFβ3 is also expressed in the lens, and has overlapping functions with TGFβ2 during lens and corneal development [71]. Since both the lens and the vasculature play a role in COL4A1-related ocular dysgenesis [74], we sought to evaluate the relative contributions of TGFβ1 and TGFβ2 by generating *Col4a1*$^{+/G1344D}$ mice that are heterozygous for a null allele of either *Tgfb1* [75] or *Tgfb2* [76]. To determine the phenotypic consequence of genetically reducing TGFβ signaling in *Col4a1*$^{+/G1344D}$ mice, we first performed slit-lamp examination at 1.3 −1.5 months of age (Fig. S9). We have demonstrated previously that the nature and severity of ASD manifestations are highly variable even in mice with the same *Col4a1* mutation [10,31]. Consistent with these findings, we observed ocular phenotypes of variable severity in *Col4a1*$^{+/G1344D}$ mice and we show that genetically reducing *Tgfb1* or *Tgfb2* levels decreased the frequency of severe ASD in *Col4a1*$^{+/G1344D}$ mice. Out of 24 *Col4a1*$^{+/G1344D}$;*Tgfb1*$^{+/+}$eyes examined, moderate and severe ASD was observed in 6 (25%) and 18 (75%) eyes, respectively (Fig. S9B). In contrast, 3 (15%), 8 (40%), and 9 (45%) out of 20 *Col4a1*$^{+/G1344D}$;*Tgfb1*$^{+/-}$ eyes examined showed mild, moderate, and severe ASD, respectively. Similarly, 1 (4%), 7 (29%), and 16 (67%) out of 24 *Col4a1*$^{+/G1344D}$;*Tgfb2*$^{+/+}$eyes examined exhibited mild, moderate, and severe ASD, respectively, compared to 3 (13%), 9 (37%), and 12 (50%) out of 24 *Col4a1*$^{+/G1344D}$;*Tgfb2*$^{+/-}$ eyes examined (Fig. S9C). We next tested whether genetic suppression of TGFβ signaling could rescue ASD in *Col4a1* mutant mice using quantifiable outcome measures including CCT (Figs. 4 and S10). OCT biometric analyses revealed that genetically reducing *Tgfb1* expression did not alter CCT in *Col4a1*$^{+/G1344D}$ mutants (Fig. 4A). However, the lens diameter was increased, while anterior chamber depth, vitreous chamber depth and axial length were reduced in *Col4a1*$^{+/G1344D}$;*Tgfb1*$^{+/-}$ mice compared to their *Col4a1*$^{+/G1344D}$;*Tgfb1*$^{+/+}$littermates (Fig. S10A,C). In contrast, while reducing *Tgfb2* gene dosage decreased CCT in *Col4a1*$^{+/+}$ mice, it lead to a small but significant increase in CCT in *Col4a1*$^{+/G1344D}$;*Tgfb2*$^{+/-}$ mice compared to *Col4a1*$^{+/G1344D}$;*Tgfb2*$^{+/+}$littermates (Fig. 4B) but did not alter the size of other ocular structures (Fig. S10B,D), and qPCR analyses confirmed that expression of TGFβ target genes was reduced in P7 anterior segments from *Col4a1*$^{+/G1344D}$;*Tgfb2*$^{+/-}$ mice compared to those from *Col4a1*$^{+/G1344D}$;*Tgfb2*$^{+/+}$littermates (Fig. 4C). Taken together, these genetic rescue experiments suggest differential roles for TGFβ1 and TGFβ2 in ocular development and disease and support the hypothesis that increased TGFβ signaling contributes to ASD in *Col4a1* mutant mice.

TGFβ neutralizing antibody has a protective effect on corneal thickness in *Col4a1*$^{+/G1344D}$ mice

Next, we tested the therapeutic potential of pharmacologically modulating TGFβ signaling to prevent ASD in *Col4a1* mutant mice. To this end, we first used the pan-TGFβ neutralizing antibody, 1D11, to reduce TGFβ signaling in *Col4a1*$^{+/G1344D}$ mice (Figs. 5 and S5). Since murine ocular development starts around E8.0 [77], mice were treated with 1D11 or control IgG1 from E8.5 to E16.5, and we measured corneal stromal thickness on histological sections at E18.5 (Fig. 5A,B). Consistent with findings from the genetic rescue experiments, 1D11 administration also significantly increased corneal stromal thickness in *Col4a1*$^{+/G1344D}$ mice compared to their IgG1-treated control counterparts (Fig. 5B). To assess if TGFβ signaling activity was

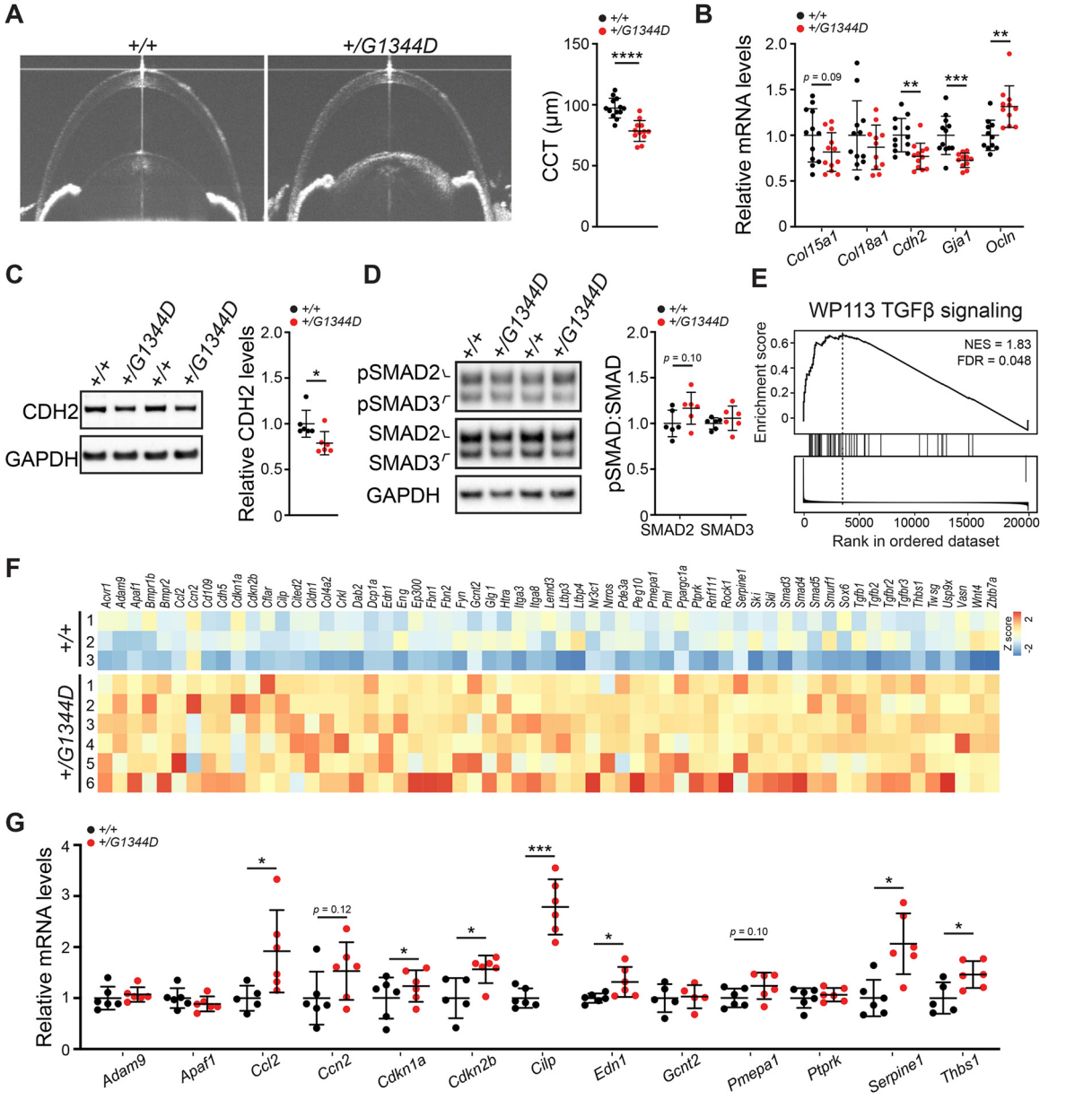

Fig. 3. *Col4a1*$^{+/G1344D}$ mice have corneal defects and increased TGFβ signaling. (**A**) Representative OCT images of anterior segments (left) and quantification (right) showing reduced CCT in *Col4a1*$^{+/G1344D}$ mice at 1.6−2.0 months of age. n = 13 *Col4a1*$^{+/+}$ and 12 *Col4a1*$^{+/G1344D}$ eyes. (**B**) qPCR analyses showing a trend towards reduced *Col15a1* expression and altered expression of corneal endothelial markers in anterior segments from P7 *Col4a1*$^{+/G1344D}$ mice compared to *Col4a1*$^{+/+}$littermates. n = 11−12 per genotype. (**C-D**) Representative Western blot images (left) and quantification (right) showing reduced CDH2 protein levels (C) and a trend towards increased pSMAD2/3:SMAD2/3 ratio (D) in anterior segments from P7 *Col4a1*$^{+/G1344D}$ compared to *Col4a1*$^{+/+}$ littermates. n = 6 per genotype. (**E**) GSEA of RNA-seq data from P0 *Col4a1*$^{+/+}$ and *Col4a1*$^{+/G1344D}$ anterior segments showing positive enrichment of the TGFβ signaling pathway (WP113). NES, normalized enrichment score; FDR, false discovery rate. (**F**) Heatmap of DEGs in the anterior segment from P0 *Col4a1*$^{+/+}$ and *Col4a1*$^{+/G1344D}$ mice contained in the enriched GO biological process "Response to transforming growth factor beta" (GO0071559). Colors representing high (red), low (blue) or average (white) expression values based on Z score normalized FPKM values for each gene. n = 3 *Col4a1*$^{+/+}$ and 6 *Col4a1*$^{+/G1344D}$ P0 anterior segment samples. (**G**) qPCR validation of selected DEGs identified by RNA-seq. n = 5−6 per genotype. Data are presented as mean ± SD. *$p < 0.05$; **$p < 0.01$; ***$p < 0.001$; ****$p < 0.0001$, Student's t-test.

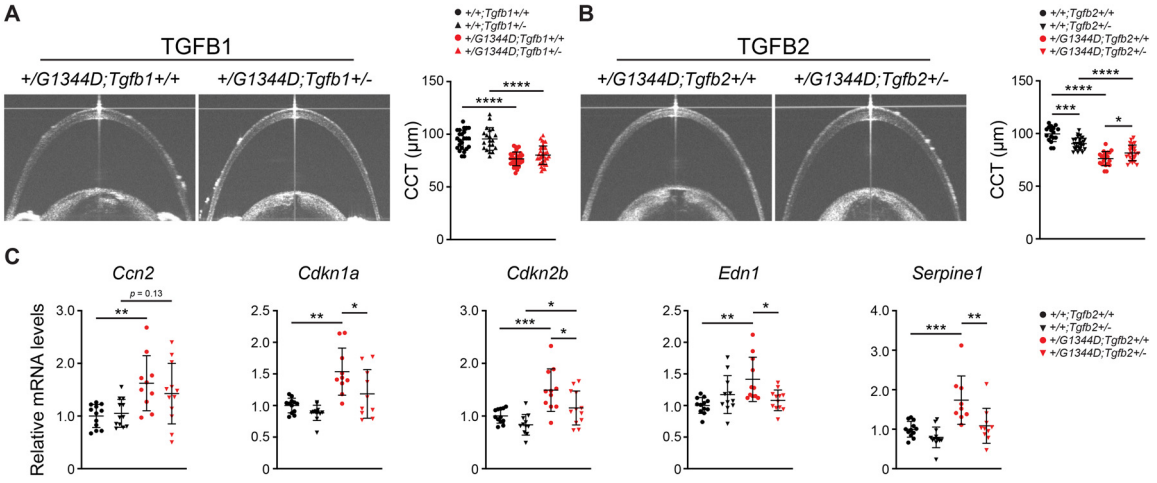

Fig. 4. Genetically reducing Tgfb2, but not Tgfb1, partially rescued corneal thickness in *Col4a1*$^{+/G1344D}$ mice. (**A**) Representative OCT images (left) and quantification (right) showing that CCT was indistinguishable between *Col4a1*$^{+/G1344D}$;*Tgfb1*$^{+/+}$and *Col4a1*$^{+/G1344D}$;*Tgfb1*$^{+/-}$ mice. n = 24 *Col4a1*$^{+/+}$;*Tgfb1*$^{+/+}$, 20 *Col4a1*$^{+/+}$;*Tgfb1*$^{+/-}$, 35 *Col4a1*$^{+/G1344D}$;*Tgfb1*$^{+/+}$, and 35 *Col4a1*$^{+/G1344D}$;*Tgfb1*$^{+/-}$ eyes. (**B**) In contrast, OCT analyses revealed that genetically reducing *Tgfb2* partially prevented CCT reduction in *Col4a1*$^{+/G1344D}$ mice. n = 17 *Col4a1*$^{+/+}$;*Tgfb2*$^{+/+}$, 27 *Col4a1*$^{+/+}$;*Tgfb2*$^{+/-}$, 20 *Col4a1*$^{+/G1344D}$;*Tgfb2*$^{+/+}$, and 25 *Col4a1*$^{+/G1344D}$;*Tgfb2*$^{+/-}$ eyes. (**C**) qPCR analyses showing increased expression of TGFβ target genes in anterior segments from P7 *Col4a1*$^{+/G1344D}$ mice that was partially prevented by genetically reducing *Tgfb2* expression. n = 9−12 samples per genotype. Data are presented as mean ± SD. *$p < 0.05$; **$p < 0.01$; ***$p < 0.001$; ****$p < 0.0001$, one-way ANOVA and Sidak's multiple comparison test.

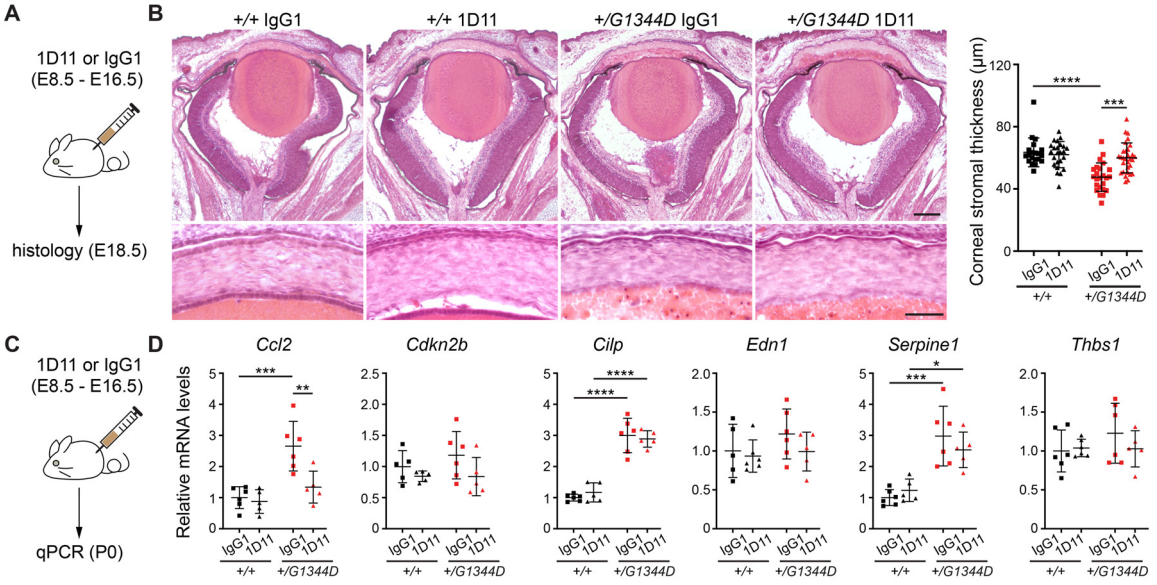

Fig. 5. 1D11 TGFβ neutralizing antibody increased corneal stromal thickness in *Col4a1*$^{+/G1344D}$ mice. (**A**) Schematic illustration of the 1D11 administration paradigm for histological analysis. (**B**) Representative images of H&E stained sections (left) showing whole eyes (top panels) and corneas (lower panels) from E18.5 mice and quantification graph (right) showing increased corneal stromal thickness in *Col4a1*$^{+/G1344D}$ mice treated with 1D11 compared to those that received the control IgG1 antibody. Scale bars = 200 μm (top) and 50 μm (bottom). n = 20 and 24 corneas from IgG1- and 1D11-treated *Col4a1*$^{+/+}$ mice, and 24 and 30 corneas from IgG1- and 1D11-treated *Col4a1*$^{+/G1344D}$ mice, respectively. (**C**) Schematic illustration of the 1D11 administration paradigm for qPCR analyses. (**D**) qPCR analyses revealed that 1D11 treatment partially prevented the increased expression of TGFβ target genes in anterior segments from P0 *Col4a1*$^{+/G1344D}$ mice compared to their IgG1-treated counterparts. n = 5−6 samples per genotype. Data are presented as mean ± SD. *$p < 0.05$; **$p < 0.01$; ***$p < 0.001$; and ****$p < 0.0001$, two-way ANOVA and Tukey's multiple comparison test.

successfully reduced by 1D11 administration, we performed qPCR analyses for a subset of TGFβ target genes. All of the target genes examined showed reduced expression in *Col4a1*$^{+/G1344D}$ mice treated with 1D11 compared to those that received IgG1; however, only the reduction in *Ccl2* expression reached statistical significance (Fig. 5C,D). Taken together, these results indicate that 1D11 administration has a protective effect in *Col4a1*$^{+/G1344D}$ mice, further supporting a causal role for altered TGFβ signaling in ASD pathogenesis in *Col4a1* mutant mice.

4PBA and losartan have protective effects on corneal stromal thickness in *Col4a1* mutant mice

The beneficial effects of 1D11 treatment on corneal thickness are an encouraging proof of concept for the therapeutic potential of pharmacologically reducing TGFβ signaling in *Col4a1* mutant mice; however, it has limited translational potential. To explore other possible therapeutic avenues, we next tested two different treatment strategies using 4-phenylbutyrate (4PBA) and losartan, two FDA-approved drugs that can be provided in drinking water, to target the proximal (protein folding and secretion) and distal (TGFβ signaling) insults in *Col4a1* mutant mice, respectively (Figs. 6 and S5). 4PBA is a small molecule with chemical chaperone properties that promotes secretion of mutant collagen α1α1α2(IV) and can theoretically simultaneously target intracellular and extracellular pathogenic events, irrespective of the nature of the extracellular insults. In contrast, losartan is an antagonist of angiotensin II type 1 receptor, which has been shown to indirectly activate SMAD signaling [78]. In theory, this may address the distal insult of increased SMAD activation without addressing

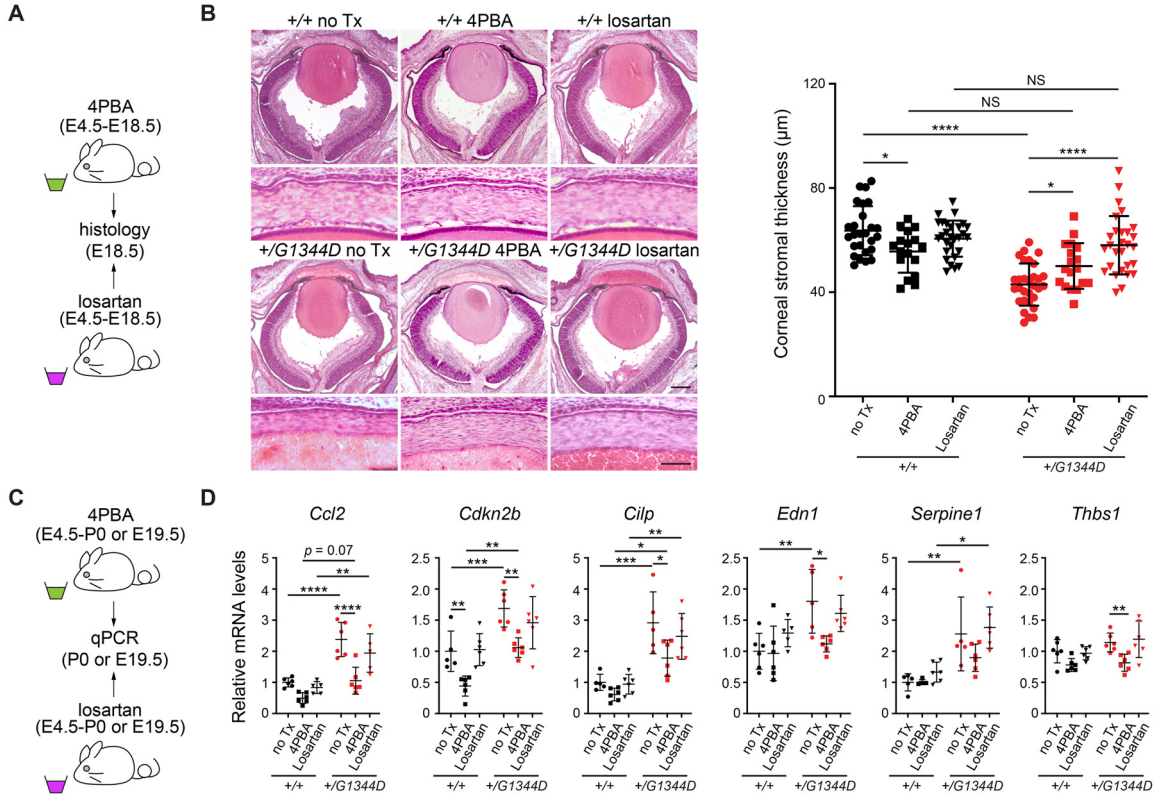

Fig. 6. Pharmacological interventions using 4PBA or losartan partially prevented the reduction in corneal stromal thickness in *Col4a1*$^{+/G1344D}$ mice. (**A**) Schematic illustration of the 4PBA and losartan treatment paradigms for histological analysis. (**B**) Representative images of H&E stained sections (left) showing whole eyes (top panels) and corneas (lower panels) from E18.5 mice and quantification graph (right) showing that 4PBA and losartan treatments both increased CCT in *Col4a1*$^{+/G1344D}$ mice. Of note, while losartan had no effect on CCT in *Col4a1*$^{+/+}$ mice, 4PBA caused a small reduction in CCT in *Col4a1*$^{+/+}$ mice. Scale bars = 200 μm (top) and 50 μm (bottom). n = 26, 17, and 28 corneas from untreated, 4PBA- and losartan-treated *Col4a1*$^{+/+}$ mice, respectively, and 30, 18, and 28 corneas from untreated, 4PBA- and losartan-treated *Col4a1*$^{+/G1344D}$ mice, respectively. (**C**) Schematic illustration of the 4PBA or losartan treatment paradigms for qPCR analyses. (**D**) qPCR analyses revealed that 4PBA, but not losartan, partially prevented the elevated expression of TGFβ target genes in anterior segments from E19.5 *Col4a1*$^{+/G1344D}$ mice. Data are presented as mean ± SD. *$p < 0.05$; **$p < 0.01$; ***$p < 0.001$; ****$p < 0.0001$; two-way ANOVA and Tukey's multiple comparison test.

collagen α1α1α2(IV) secretion defects. We have previously demonstrated that 50 mM 4PBA treatment ameliorates cerebrovascular and neuromuscular pathologies in *Col4a1*$^{+/\Delta ex41}$ mice [34,35,79]. In contrast, in a pilot study we found that providing pregnant dams with 50 mM 4PBA did not reduce ASD severity in *Col4a1*$^{+/\Delta ex41}$ mice (data not shown). Higher concentrations of 4PBA (100 mM) had beneficial effects on skeletal myopathy and intracerebral hemorrhages when provided after weaning, but led to dystocia and adverse maternal nurturing behavior leading to perinatal death when providing earlier [79]. We reasoned that the eye may be less accessible to 4PBA, and thus we provided pregnant dams with 100 mM 4PBA from E4.5 to E18.5 when corneal stromal thickness was assessed, or from E4.5 to E19.5 when pups were surgically delivered and used for molecular analyses. We found that while 100 mM 4PBA treatment caused a small but significant decrease in corneal stromal thickness in *Col4a1*$^{+/+}$ mice, it significantly increased corneal stromal thickness in *Col4a1*$^{+/G1344D}$ mice (Fig. 6A,B). Moreover, 4PBA administration normalized TGFβ target gene expression in anterior segments from E19.5 *Col4a1*$^{+/G1344D}$ embryos (Fig. 6C,D). Despite the significant contraindications for embryonic use, these findings demonstrate that 4PBA can ameliorate ocular dysgenesis in *Col4a1* mutant mice and support a model where elevated TGFβ signaling represent a distal insult acting downstream of extracellular α1α1α2(IV) deficiency.

Next, we used losartan as a mechanism-based intervention to target increased SMAD activation as a distal insult contributing to ASD in *Col4a1* mutant mice. To this end, pregnant dams were provided with losartan in drinking water from E4.5 to E18.5 when corneal stromal thickness was assessed (Fig. 6A,B). Losartan treatment resulted in a significant improvement in corneal stromal thickness in *Col4a1*$^{+/G1344D}$ mice compared to their untreated counterparts. Interestingly, we did not detect an effect of losartan on the expression of TGFβ target genes in anterior segments from P0 *Col4a1*$^{+/G1344D}$ mice (Fig. 6C,D) suggesting that the protective effect of losartan may not be mediated by modulation of the selected genes. Notably, however, despite having beneficial effect on CCT in *Col4a1* mutant mice, gestational administration of losartan was also associated with increased postnatal death (Table S1) precluding it from being a viable treatment approach.

Since 4PBA and losartan treatments both improve CCT in *Col4a1*$^{+/G1344D}$ mice, we applied these approaches to two additional *Col4a1* mutant strains – *Col4a1*$^{\Delta ex41}$ and *Col4a1*^{G394V} (Fig. S11). As previously described, *Col4a1*^{G1344D} represents a glycine missense mutation whereas *Col4a1*$^{\Delta ex41}$ has a deletion of 17 amino acids resulting from a skipped exon. The *Col4a1*^{G394V} mutation is also a glycine missense mutation; however, the ASD and cerebrovascular phenotypes are less severe in *Col4a1*$^{+/G394V}$ mice compared to *Col4a1*$^{+/G1344D}$ *and* *Col4a1*$^{+/\Delta ex41}$ mice [33,34]. Similar to what we observed in *Col4a1*$^{+/G1344D}$ and *Col4a1*$^{+/\Delta ex41}$ mice, histological analysis revealed a significant reduction in corneal stromal thickness in untreated *Col4a1*$^{+/G394V}$ mice compared to their respective *Col4a1*$^{+/+}$ littermates (Fig. S11). Importantly, while 4PBA treatment lead to slightly thinner corneas in wildtype littermates, it improved corneal stromal thickness in *Col4a1*$^{+/\Delta ex41}$ and *Col4a1*$^{+/G394V}$ eyes compared to their untreated counterparts; however, statistical significance was only observed for *Col4a1*$^{+/G394V}$ eyes. While losartan had no effect on corneal thickness in *Col4a1*$^{+/+}$and *Col4a1*$^{+/\Delta ex41}$ mice, CCT was comparable between losartan-treated *Col4a1*$^{+/G394V}$ mice and their *Col4a1*$^{+/+}$littermates, and a trend toward increased corneal thickness was observed in losartan-treated *Col4a1*$^{+/G394V}$ mice compared to their untreated counterparts (Fig. S11). Collectively, these findings indicate that 4PBA and losartan both have protective effects on CCT in *Col4a1* mutant mice and highlight the importance of the TGFβ signaling pathway in *Col4a1*-related pathology. However, dystocia and perinatal lethality associated with embryonic administration of 100 mM 4PBA or losartan underscore that these treatment strategies are not viable therapeutic options and approaches to specifically target the TGFβ signaling pathway in the eye without causing systemic detrimental effects will need to be explored.

Discussion

Type IV collagens are fundamental BM components and mutations in *COL4A1* and *COL4A2* cause Gould syndrome, a genetic disorder that typically presents as a constellation of variable manifestations affecting multiple organ systems [9,80]. After cerebrovascular defects, ocular abnormalities, including ASD and glaucoma, are the most frequently reported clinical findings in individuals with Gould syndrome [14,24]. Notably, pathogenic *Col4a1* and *Col4a2* mutations were first identified using forward mutagenesis screens in mice with variable forms of ocular pathology, and *Col4a1* and *Col4a2* mutant mice represent valuable pre-clinical models to study Gould syndrome [25–33]. Despite the increasing recognition of Gould syndrome as a clinical entity and the advances made in understanding this multisystemic disorder in recent years, the molecular mechanisms by which *COL4A1* and *COL4A2* mutations lead to disease remain elusive. In this study, we show that TGFβ signaling is elevated in developing ocular anterior segments from

Col4a1 mutant mice and demonstrate that genetically or pharmacologically reducing TGFβ signaling partially rescued ocular dysgenesis. These data suggest that elevated TGFβ signaling represents an important pathogenic mechanism contributing to ASD and possibly other aspects of Gould syndrome. These findings have broad implications for understanding the basic biological functions of type IV collagens and for the development of therapeutic interventions for clinical manifestations associated with Gould syndrome.

Here we show that, in addition to previously reported ocular features [30–33], reduced corneal thickness is an early morphological defect in *Col4a1* mutant mice that persists through adulthood. Notably, in addition to ASD [81], corneal thinning is associated with other ocular diseases such as keratoconus and primary open angle glaucoma, as well as with connective tissue disorders including Marfan [82] and Ehlers-Danlos syndromes [83]. The corneal stroma is the major determinant of corneal thickness and is mainly composed of sparsely dispersed corneal keratocytes and orthogonally arranged layers of collagen fibrils. Thus, we predicted that thin corneas might be due to decreased numbers of keratocytes or reduced production of the stromal ECM but we did not detect differences in the number of corneal stromal cells or expression levels of genes coding for major ECM proteins. Ultrastructural analyses revealed reduced diameter and increased density of collagen fibrils in the corneal stroma of *Col4a1* mutant mice as well as thinner and denser collagen lamellae. Consistent with a fundamental role of collagen α1α1α2(IV) in BM integrity, we also observed focal disruption of the epithelial BM and thinner Descemet's membrane. The mechanism(s) underlying corneal morphological changes in *Col4a1* mutant mice are unclear, and future studies using more detailed biochemical and biomechanical approaches may help to determine the pathogenic processes involved. Irrespective of the underlying mechanism(s), corneal thickness is a quantitative trait that represent a useful tool to assess ASD severity.

Development of the anterior segment is a complex process and involves tissues of four different embryonic origins. Surface ectoderm gives rise to the lens and corneal epithelium, while the neural ectoderm give rise to the retina and pigmented epithelia of the iris and ciliary body. The periocular mesenchyme, which consists of neural crest and mesodermal cells, gives rise to the majority of the anterior segment structures including corneal stroma and endothelium, iris and ciliary stroma, and ocular drainage structures [77,84]. Corneal stromal and endothelial abnormalities observed in *Col4a1* mutant mice suggest potential defects in periocular mesenchyme differentiation. FOXC1 and PITX2 are transcription factors that are critical for periocular mesenchyme development, and *FOXC1* and *PITX2* mutations are among the most common causes of ASD and developmental glaucoma [2]. Interestingly, animal studies show that FOXC1 is also required for cerebral vascular development, and some patients with *FOXC1* and *PITX2* mutations have cerebral small vessel disease, which is a central manifestation of Gould syndrome [85–87], suggesting that COL4A1, FOXC1, and PITX2 may participate in overlapping pathways. In *Col4a1*$^{+/\Delta ex41}$ mice that have severe ASD, we observed a modest reduction in the expression of genes associated with the FOXC1 and PITX2 regulatory networks, but this observation was not validated in a second milder strain. However, because of the tissue scarcity and cellular heterogeneity of embryonic and early postnatal anterior segment structures these molecular approaches are technically challenging. It is possible that subtle changes in these pathways are indeed involved but that we lack the sensitivity or temporal resolution to detect them, thus, the potential roles of FOXC1 and/or PITX2 transcriptional networks in ASD pathogenesis in *Col4a1* mutant mice remains equivocal.

We previously demonstrated that 50 mM 4PBA promoted collagen α1α1α2(IV) secretion and reduced intracerebral hemorrhage and myopathy severity in *Col4a1* mutant mice [34,35,79]. Here we show that 4PBA treatment at a higher dose (100 mM) could also partially rescue corneal thickness in *Col4a1* mutant mice. Interestingly, another study reported that 4PBA administration ameliorated ICH but not ocular pathology in a distinct *Col4a1* mutant mouse model [88]. The discrepancy between these studies might be explained by differences in phenotyping approaches, the specific mutant allele involved, or treatment dosages (1 g/kg/day in the previous report). In support of this notion, in a pilot experiment we found that 50 mM 4PBA was unable to reduce corneal thickness in *Col4a1* mutant mice suggesting the eye may be less accessible or have a higher threshold for efficacy. However, provision of 100 mM 4PBA during embryogenesis caused dystocia and affected maternal nurturing behavior [79], precluding evaluation of postnatal mice.

TGFβ superfamily members are pleiotropic cytokines involved in the regulation of multiple cellular processes, including those involved in anterior segment formation. Because loss of function mutations in *BMP4* and *BMP7* cause ASD in humans [55,56] and type IV collagens can regulate the signaling strength and range of Dpp (a BMP ortholog) in *Drosophila* [41,43], we predicted that *Col4a1* mice might have altered BMP signaling. However, we found no evidence to support this hypothesis. In contrast, using a combination of independent hypothesis-driven and unbiased approaches, we show that canonical TGFβ signaling is elevated in *Col4a1* mutant mice. The strongest evidence supporting a causative role for elevated TGFβ signaling in ASD in *Col4a1* mutant mice is the observation that corneal

thickness can be partially rescued by reducing gene dosage of *Tgfb2* – the major ligand isoform in developing eyes. Interestingly, our data also indicate that TGFβ1 and TGFβ2 have distinct roles in ocular development. Genetically reducing *Tgfb1* levels rescued anterior chamber depth, lens diameter and vitreous chamber depth, but not CCT, whereas genetically reducing *Tgfb2* rescued CCT but not the other ocular parameters. These data suggest that, while TGFβ2 may be the major ligand involved in corneal development, TGFβ1 is involved in other aspects of ocular development and that *Col4a1* mutations influence both TGFβ1- and TGFβ2-mediated processes. Of note, *Tgfb2* heterozygosity only partially rescued CCT suggesting that other mechanisms might also be involved. Collectively, these findings support that elevated TGFβ signaling is a key pathogenic consequence of reduced collagen α1α1α2(IV) secretion in *Col4a1* mutant mice.

To test TGFβ signaling as a potential therapeutic target, we treated *Col4a1* mutant mice with the 1D11 pan-TGFβ neutralizing antibody which blocks activity of all three TGFβ ligands. In support of our hypothesis, embryonic 1D11 administration rescued corneal thickness in *Col4a1*$^{+/G1344D}$ mice and reduced expression levels of several canonical TGFβ target genes. However, in contrast to 4PBA provision that significantly reduced the expression of 5 out of the 6 TGFβ target genes tested, only one target gene reached statistical significance following 1D11 administration. A possible explanation is that promoting α1α1α2(IV) secretion via continuous 4PBA treatment has effects that are both persistent and diverse if the heterotrimers polymerize into a stable network and execute multiple extracellular functions. In contrast, 1D11 may have achieved suppression of target genes during a critical developmental period allowing a partial phenotypic rescue but cannot sustain suppression at the ages tested because of the intermittent 1D11 injection and short circulatory half-life (34 h) [89]. Alternatively, we have not exhaustively addressed the roles of canonical and non-canonical signaling or related pathways and the target genes that we selected may not be the key effectors for anterior segment development. Although we did not find evidence for the involvement of the ERK and p38 MAP kinase pathways, other non-canonical pathways remain to be tested and detailed studies using more sensitive analyses at multiple developmental stages might be required.

Elevated TGFβ signaling has been implicated in the pathogenesis of Marfan syndrome, a prototypical ECM disorder caused by Fibrillin 1 (*Fbn1*) mutation [90–93]. The role for TGFβ signaling in Marfan syndrome is complex and although clinical trials using losartan to indirectly suppresses excess TGFβ signaling have given inconsistent results [94,95], losartan improved clinically-relevant pathology in mouse models of Marfan syndrome [90,96–100]. Individuals with Marfan syndrome also have thin corneas and we tested whether losartan administration could rescue ocular dysgenesis and corneal thickness in *Col4a1* mutant mice. Because ocular development begins at mid-gestation, we administered losartan prenatally despite its contraindication during pregnancy [101]. Indeed, embryonic losartan administration caused early postnatal lethality, which diminishes prospects for therapeutic potential; however, corneal thickness at E18.5 was rescued in *Col4a1*$^{+/G1344D}$ and *Col4a1*$^{+/G394V}$ mice. In contrast, no beneficial effect of losartan was observed in *Col4a1*$^{+/\Delta ex41}$ mice, suggesting a different dose or dosing regimen might be needed in mice with more severe pathology. Similar observations were reported in mouse models of Marfan syndrome in which losartan displays no or moderate protective effect in more severe models [96,98,100]. In contrast to 1D11, expression levels of selected TGFβ target genes were not reduced by losartan, suggesting that other target genes or downstream mechanisms may be involved. Notably, the protective effect of losartan in Marfan syndrome was mainly attributed to suppression of ERK signaling [78,92,93]. However, the angiotensin II type I receptor, the direct target of losartan, can signal through multiple pathways and modulate multiple pathophysiological functions [102] and the mechanism underlying the protective effect of losartan on CCT in *Col4a1* mutant mice remains to be determined.

While the data presented in this study demonstrate a causal relationship between altered TGFβ signaling and ocular pathology in *Col4a1* mutant mice, the specific molecular and cellular processes involved have yet to be defined. First, it is unclear how *Col4a1* mutations lead to elevated TGFβ signaling. Evidence that TGFβs and BMPs bind directly to type IV collagens may lend support to a mechanism whereby extracellular collagen α1α1α2(IV) deficiency leads to increased TGFβ ligand bioavailability, similar to the mechanism proposed for Marfan syndrome [91]. TGFβ2 is highly expressed in the developing lens, and both the lens capsule and Descemet's membrane are thick BMs that are capable of sequestering growth factors. It is possible that reduced levels of collagen α1α1α2(IV) in those BMs could increase TGFβ bioavailability. In support of this, we previously showed that lens-specific expression of mutant *Col4a1* caused ASD in a dose-dependent manner [74]. Alternatively, collagen α1α1α2(IV) contains multiple consensus binding sites for integrins α1β1 and α2β1 [103–105], and integrin α1β1 activation can suppress TGFβ signaling by inhibiting TGFBR2 receptor activity [106]. Thus, reduced levels of extracellular collagen α1α1α2(IV) might lead to de-repression of TGFβ signaling through decreased integrin α1β1 activity. Furthermore, heparan sulfate deficiency in neural crest-derived tissues also lead to elevated TGFβ signaling and ASD [107], raising the possibility that *Col4a1* mutations

could affect TGFβ signaling indirectly through other ECM molecules. Complicating attempts to identify the molecular mechanism is the fact that anterior segment morphogenesis is a complex multistep process involving highly coordinated interactions between multiple tissues and it is still not clear which cell types are responsible for aberrant TGFβ signaling and at which developmental stages. Conditional gene targeting approaches might help determining the spaciotemporal involvement of TGFβ signaling in COL4A1-mediated anterior segment development and dysgenesis.

Key findings of this study are that the type IV collagen network regulates TGFβ signaling and that elevated TGFβ signaling is a pathogenic mechanism contributing to COL4A1-related ocular dysgenesis. However, the partial protective effects seen in the genetic and pharmacological rescue experiments suggest the contribution of additional pathogenic mechanisms. Supporting this possibility, RNA-seq analysis also highlighted functional terms such as "cell-matrix adhesion" and "focal adhesion" which have been implicated in various cellular processes central to ocular development and disease, including mechanical signal transduction, cell survival, migration and differentiation [108–111]. Enrichment for GO terms and pathways that have been linked to ECM responsiveness including "mitochondrion organization", "electron transport chain", and "oxidative phosphorylation" was also observed [112]. Moreover, accumulating evidence suggests that the type IV collagen network acts as a multifunctional signaling platform and *in vivo* and *in vitro* studies have identified diverse biological functions including acting as ligands for G protein-coupled receptors [37,113,114] or regulating guidance cues such as Netrin-1 and Slit [115,116]. In addition to regulating cell signaling, type IV collagens also play a central role in BM assembly and organization which is critical for embryonic development and tissue morphogenesis, including eye formation [31,117–119]. In light of the diverse and multifunctional roles of type IV collagens and complexity of ocular development, additional pathological processes are likely to act in concert with elevated TGFβ signaling to cause ASD in *Col4a1* mutant mice.

Although analyses presented in this study focused on development, chronically increased TGFβ signaling may also contribute to other progressive ocular defects observed in *Col4a1* mutant mice. For instance, *Col4a1* mutations in mice cause glaucoma [30,32] which is also observed in a subset of individuals with Gould syndrome [120–125]. Increased levels of TGFβ ligands were reported in the aqueous humor and optic nerve heads of glaucomatous eyes [126–130]. Increased TGFβ signaling can modulate cell contractility and ECM turnover in the trabecular meshwork, influencing aqueous humor outflow and intraocular pressure, and can induce changes at the optic nerve head and cause axon damage [128–130]. Thus, it is possible that chronically increased TGFβ signaling in *Col4a1* mutants could also impair homeostasis of ocular drainage tissues leading to progressive intraocular pressure elevation and glaucoma. Finally, aberrant TGFβ signaling has well-established and important roles in other clinical manifestations commonly associated with Gould syndrome, including renal fibrosis and vascular diseases [131,132], suggesting that elevated TGFβ signaling might represent a pathogenic mechanism contributing to various aspects of the syndrome.

Collectively, the findings presented in this study establish a functional role for type IV collagens in TGFβ signaling regulation and identify elevated TGFβ signaling as a novel and clinically-relevant mechanism contributing to ocular dysgenesis in *Col4a1* mutant mice. A logical extension of our findings predicts that elevated TGFβ signaling may be generally important across many organs affected in Gould syndrome and potentially in Alport syndrome [133] which is also caused by mutations in genes encoding type IV collagens. If our findings are validated in other organs and in individuals with Gould syndrome, TGFβ signaling might represent a novel therapeutic target.

Experimental procedures

Animals

All experiments were conducted in compliance with the ARVO Statement for the Use of Animals in Ophthalmic and Vision Research and approved by the Institutional Animal Care and Use Committee at the University of California, San Francisco (Protocols AN159737 and AN182181). *Col4a1* mutant mouse strains have been described previously [25,27,33]. All *Col4a1* mutant mice used in this study were heterozygous and backcrossed to C57BL/6J (B6) mice for at least 17 generations. TGFβ signaling reporter mice (*SBE-Luc* mice) that express luciferase in response to SMAD2/3-mediated TGFβ signaling [64], *Tgfb1*$^{+/-}$ [75] and *Tgfb2*$^{+/-}$ [76] mice were iteratively crossed to B6 mice for at least five generations and bred to *Col4a1*$^{+/mut}$ mice to generate *Col4a1*$^{+/mut}$ and *Col4a1*$^{+/+}$ littermates heterozygous for the *Tgfb1 or Tgfb2* null mutation or carrying the *SBE-luc* reporter transgene. All animals were maintained in full-barrier facilities free of pathogens on a 12 h light/dark cycle with ad libitum access to food and water. Both male and female mice were used for all experiments and no samples were excluded from the study.

Histological analyses and corneal stromal thickness quantification

Heads from E18.5 embryos were fixed in 4% paraformaldehyde (PFA) in phosphate buffered

saline (PBS) overnight at 4 °C, cryoprotected in 30% sucrose/PBS, and embedded in optimal cutting temperature compound (Sakura Finetek, Torrance, CA). Coronal sections (12 μm) were prepared using a Leica CM1900 cryostat (Rankin Biomedical Corp. Holly, MI) and sections at the level of the optic nerve head were selected, stained with hematoxylin and eosin (H&E), and imaged for quantification of central corneal stromal thickness defined as the distance between the corneal epithelium and corneal endothelium.

Ocular biometry by optical coherence tomography (OCT)

Ocular biometry was performed using Envisu R4300 spectral-domain optical coherence tomography (SD-OCT, Leica/Bioptigen Inc., Research Triangle Park, NC, USA) as previously described [134]. Briefly, mice were anesthetized using ketamine/xylazine (100 mg/kg and 50 mg/kg, respectively) and their pupils were dilated with 0.5% Tropicamide and 0.5% phenylephrine hydrochloride. Artificial tears (Genteal, Alcon, Fort Worth, TX) were applied onto the cornea to maintain hydration and transparency during imaging. Eyes were positioned so that the laser beam passes along the optical axis and correct alignment was achieved by placing the Purkinje image in the center of the pupil. Rectangular volume and radial volume scans were performed to capture images for retinal thickness and axial length measurements, respectively. Various ocular parameters were measured including central corneal thickness, ocular axial length, anterior chamber depth, vitreous chamber depth, lens diameter and retinal thickness.

Transmission electron microscopy (TEM)

Intact eyes from P0 and 2.5 months old mice were fixed in 1.5% paraformaldehyde/1.5% glutaraldehyde (Electron Microscopy Sciences, #15950) with 0.05% tannic acid in DMEM for two hours, after which the interior of the globes were exposed to fixative via shallow scleral piercings. Following glutaraldehyde immersion for two days, the globes were rinsed in DMEM, then bisected using a double-edge razor blade. Tissues were post-fixed in 1% OsO_4 overnight, then dehydrated in a graded series of ethanol to 100%, rinsed in propylene oxide, extensively infiltrated in Spurr's epoxy, then embedded and polymerized at 70 °C for 18 h. Eighty-nanometer ultrathin sections were cut on a Leica EM UC7 ultramicrotome (Leica Microsystems) and mounted on formvar-coated 1 × 2 mm slot grids. Grids were stained in uranyl acetate followed by lead citrate, then imaged using a FEI G2 TEM operated at 120 KV. Images were collected using an AMT 2K × 2K side entry digital camera (AMT, Woburn, MA).

Fibril diameter and density measurements

Two series of 15−22 images, spanning from corneal epithelium to the endothelium, were taken at 50,000x from two different locations. Regions of interest (ROIs) containing mostly cross-sectioned collagen fibrils were randomly selected from each image. The number and cross-sectional area of fibrils were measured using Fiji (National Institutes of Health (NIH)). Fibril diameters were calculated from cross-sectional areas after calibration. To plot the distribution curve, measurements for fibrils from mice with the same age and genotype (n = 3 per group) were combined. Total fibrils measured were 7393 and 9558 for P0 *Col4a1*$^{+/+}$ and *Col4a1*$^{+/\Delta ex41}$ mice, respectively, and 11,676 and 12,402 for 2.5 months old *Col4a1*$^{+/+}$ and *Col4a1*$^{+/\Delta ex41}$ mice, respectively. The total fibril number and the area for each ROI were recorded to calculate fibril density. The mean fibril density for each sample were averaged from all ROIs from the same image series.

Slit-lamp biomicroscopy

Ocular anterior segment examinations were performed on 1.3−1.5 months old mice using a slit-lamp biomicroscope (Topcon SL-D7; Topcon Medical Systems, Oakland, NJ, USA) attached to a digital SLR camera (Nikon D200; Nikon, Melville, NY, USA). ASD severity was determined based on the level of iris vessel dilation and tortuosity, pupil dilation, lens opacity and anterior chamber enlargement as previously described [10].

RNA extraction and quantitative polymerase chain reaction (qPCR)

Ocular tissues including whole eyes or anterior segments were stabilized in RNAlater (ThermoFisher Scientific, USA) and stored at −80 °C until use. Anterior segments were dissected in PBS by cutting along the limbus with scissors. After removing the lens, the remaining anterior segment (cornea, iris, ciliary body and ocular drainage structures) was collected. Embryonic and early postnatal samples were pooled with 4 eyes from 2 mice (E14.5 and P0) and 2 eyes from 1 mouse for P7 anterior segments. Total RNA was extracted using the RNeasy Plus Micro kit (Qiagen, Germantown, MD) according to the manufacturer's instructions. RNA was reverse transcribed to cDNA using iScript cDNA synthesis kit (Bio-Rad, Hercules, CA). Quantitative PCR was performed on a Bio-Rad CFX96 real-time system using SsoFast Evagreen mix (Bio-Rad) and primers listed in Table S2. Briefly, 10 ng of cDNA and 1.25 μM primers were used per reaction in a final volume of 10 μl. Each cycle consisted of denaturation at 95 °C for 5 s, followed by annealing and extension at 60 °C for 5 s for a total of 45 cycles.

All experiments were run with technical duplicates and at least 4 biological replicates were used per group. The relative expression of each gene was normalized to *Hprt1* or *Gapdh* and analyzed using the $2^{-\Delta\Delta CT}$ method [135].

RNA-sequencing and data analysis

Four anterior segments from 2 P0 mice of the same genotype were pooled for RNA purification with RNeasy Plus Micro kit (Qiagen). RNA quality assessment, library preparation, sequencing and bioinformatic analysis were performed by Novogene Inc. (Sacramento, CA). Briefly, RNA quality was determined using an Agilent Bioanalyzer, and samples with RNA integrity number (RIN) scores >9.0 were further processed. Illumina sequencing libraries were prepared and sequenced (150 bp pair-ended) on an Illumina Novaseq6000 sequencer. Raw reads were trimmed and filtered to remove the adaptor sequence and low-quality reads. Filtered reads were aligned to mouse reference genome assembly (GRCm38) using STAR v2.6.1 and the read count table was generated using HTseq v0.6.1. Fragments per kilobase of transcript sequence per million mapped reads (FPKM) >1 were used as a threshold for gene expression. Differential gene expression analysis was performed using the DEseq2 v1.6.3 R package and *p* values were adjusted using the Benjamini-Hochberg method. Differentially expressed genes (DEGs) were defined by having adjusted *p* values of less than 0.05. Over-representation analysis including gene ontology (GO) enrichment analysis was implemented using the clusterProfiler v2.4.3 R package [136]. GO terms with corrected *p* values < 0.05 were considered significantly enriched. Gene set enrichment analysis (GSEA) were performed using WebGestalt v2019 [137,138] and molecular pathways collected in Wikipathways as a functional database [139,140]. Pathways with a false discovery rate (FDR) < 0.05 were considered significantly enriched. The RNA-seq data in this study was deposited at Gene Expression Omnibus (GEO) (http://www.ncbi.nlm.nih.gov/geo/) under accession ID GSE202801.

Immunofluorescence labeling

Heads from E18.5 embryos were fixed in 4% PFA in PBS overnight at 4 °C, cryoprotected in 30% sucrose in PBS, and embedded in optimal cutting temperature compound. Coronal cryosections (12 μm) were prepared as described for histological analyses. For pSMAD2 immunolabeling, sections were boiled in 10 mM citrate buffer pH 6.0 for 20 min for antigen retrieval, blocked in PBS containing 1% Triton X-100 (PBST), 10% normal donkey serum and 1% BSA, and incubated with rabbit anti-pSMAD2 antibody (Cell Signaling #3101, 1:100) in blocking buffer at 4 °C overnight. Then, sections were washed in PBST and incubated in species-specific Alexa Fluor 488- or 594- conjugated secondary antibodies (ThermoFisher Scientific, 1:500) for 1 h at room temperature, counterstained with DAPI (1 μg/ml), mounted in Prolong Gold Antifade Mountant (ThermoFisher Scientific) and imaged using a Zeiss LSM700 confocal microscope equipped with a Plan-Apochromat 63x/1.40 objective and ZEN software (Carl Zeiss Microscopy). Fluorescence intensity of nuclear pSMAD2 labeling was quantified using Fiji (NIH). Briefly, DAPI staining was used to create a ROI containing nuclei. Nuclear ROI was then applied to the original pSMAD2 labeling images and the mean pixel intensities were recorded and compared between genotypes. The number of nuclei in the corneal stroma was quantified by counting the number of DAPI positive particles in a 100 μm segment of the central corneal stroma.

Immunolabeling of corneal whole mounts were performed as previously described with some modifications [141]. Briefly, mouse corneas were dissected and fixed in 0.5% PFA in PBS for 30 min at room temperature. Corneas were blocked in PBS containing 1% Triton X-100, 0.1% Tween-20, 10% normal donkey serum and 3% BSA for 1 h at room temperature and incubated with rabbit anti-CDH2 antibody (Cell Signaling #13116, 1:500) in blocking buffer for 48 h at 4 °C. Following washes in PBS, corneas were incubated in species-specific Alexa Fluor 488- or 594- conjugated secondary antibodies (ThermoFisher Scientific, 1:1000) and DAPI (0.2 μg/ml) at 4 °C overnight before mounting. Corneas were imaged using the Zeiss LSM700 confocal. Z-stack images covering the entire corneal endothelium were condensed to two-dimensional images in Fiji using the standard deviation method in the Z-projection function.

Western blot analyses

Both anterior segments from one P7 mouse were pooled as one sample. Samples were homogenized on ice in T-PER buffer (ThermoFisher Scientific, USA) supplemented with Halt Protease and Phosphatase Inhibitor Cocktail (ThermoFisher Scientific), EDTA and 2 mM phenylmethylsulfonyl fluoride using a disposable pestle. Total protein concentrations were measured using the bicinchoninic acid (BCA) assay kit (ThermoFisher Scientific), and 6 μg of proteins was separated on Bolt 4−12% Bris Tris Plus gels under reducing conditions and transferred onto polyvinylidene difluoride membranes (Bio-Rad). Membranes were blocked in 10% BSA or 5% milk in TBST (TBS with 0.1% Tween-20) for 2 h at room temperature or overnight at 4 °C and incubated with primary antibodies diluted in 5% BSA or 2% milk at 4 °C overnight. Dilutions of primary antibodies used

in this study are as follows: rabbit anti-pSMAD2 (Cell Signaling #3101, 1:1000), rabbit anti-SMAD2 (Cell Signaling #5339, 1:1000), rabbit anti-pSMAD3 (Abcam #ab52903, 1:1000), rabbit anti-SMAD2/3 (Cell Signaling #8685, 1:1000), rabbit anti-pSMAD1/5/9 (Cell Signaling #13820, 1:1000), rabbit anti-SMAD1/5/9 (Santa Cruz #sc-6031-R, 1:500), rabbit anti-pP38 MAPK (Cell Signaling #9211, 1:1000), rabbit anti-P38α MAPK (Cell Signaling #9218, 1:1000), rabbit anti-pERK1/2 (Cell Signaling #9101, 1:1000), rabbit anti-ERK1/2 (Cell Signaling #4695, 1:1000), rabbit anti-CDH2 (Cell Signaling #13116, 1:1000) and mouse anti-GAPDH (Millipore #MAB374, 1:100000). Following washes in TBST, membranes were incubated with secondary horseradish peroxidase-conjugated donkey anti-rabbit (Jackson Immuno Research Laboratories #711-035-152, 1:10000) or anti-mouse antibodies (Jackson Immuno Research Laboratories #715-035-150, 1:10000) for 1 h at room temperature. Immunoreactivity was visualized using chemiluminescence (ECL or Luminata Forte substrate, ThermoFisher Scientific) and imaged with the ChemiDoc MP Imaging System (Bio-Rad) or exposed to X-ray films. Restore Plus Stripping buffer (ThermoFisher Scientific) was used to strip membranes that were probed with different antibodies raised in the same species. Densitometric analyses were performed on low exposure images using the Quantity One software (Bio-Rad).

Luciferase activity assay

Both anterior segments from one P7 mouse were pooled as one sample. Samples were homogenized in Glo lysis buffer (Promega, Madison, WI), incubated for 1 h at 4 °C and the supernatant was collected by centrifugation. Luciferase activity was measured using the One-Glo Luciferase assay system (Promega) and a Veritas Microplate Luminometer (Promega). Total protein concentration was determined using the BCA assay and luciferase activity was normalized to total protein concentration.

1D11 TGFβ neutralizing antibody treatment

Timed-pregnant B6 females crossed with *Col4a1*$^{+/G1344D}$ males were injected intraperitoneally with the 1D11 pan-TGFβ neutralizing antibody (clone 1D11.16.8, BioXCell, West Lebanon, NH) or IgG1 isotype control antibody (clone MOPC-21, BioXCell) diluted in inVivoPure Dilution Buffer (pH 7.0, BioXCell) (20 mg/kg) every other day from E8.5 to E16.5 and animals were harvested at E18.5 or P0 for histological and molecular analyses, respectively.

4PBA and losartan treatments

Timed-pregnant B6 females crossed with *Col4a1*$^{+/G1344D}$ males were provided continuously with 100 mM 4PBA (Scandinavian Formulas) or 0.6 g/L losartan (Aros Organics or TCI America) in drinking water starting from E4.5 and tissues from the progeny were collected at E18.5 for corneal stromal thickness measurement or E19.5/P0 for qPCR analysis, respectively.

Statistics

Statistical analyses were performed using GraphPad Prism v8.0 (GraphPad, La Jolla, CA). Statistical differences between two groups were determined using two-tailed unpaired Student's t-test or Mann-Whitney test. Multiple-group comparisons were performed using one-way ANOVA and Sidak's multiple comparison test. To evaluate the effect of treatment among various genotypes, two-way ANOVA and Tukey's multiple comparison test were used. Differences in distribution were analyzed using Kolmogorov-Smirnov test. Data are presented as mean± SD and p values < 0.05 were considered statistically significant.

CRediT authorship contribution statement

Mao Mao: Conceptualization, Methodology, Investigation, Visualization, Funding acquisition, Writing – original draft, Writing – review & editing. **Cassandre Labelle-Dumais:** Conceptualization, Writing – original draft, Writing – review & editing. **Sara F. Tufa:** Methodology, Writing – review & editing. **Douglas R. Keene:** Methodology, Writing – review & editing. **Douglas B. Gould:** Conceptualization, Investigation, Funding acquisition, Supervision, Writing – original draft, Writing – review & editing.

Declaration of Competing Interest

The authors declare no conflicts of interest.

Acknowledgments

We thank Drs. Seyyedhassan Paylakhi, Swanand Koli and Saidas Nair for guidance with OCT imaging. We thank Dr. Tamara Alliston for providing p38 antibodies and *SBE-luc* reporter mice and Dr. Eric Ullian for providing the pERK1/2 antibody. We thank Dr. Mary Barcello-Hoff for providing *Tgfb1*$^{+/-}$ mice, and Dr. Mohamad Azhar for providing *Tgfb2*$^{+/-}$ mice. We also thank the UCSF Center for Advanced

Technology and Parnassus Garage for Advanced Technologies for use of shared equipment.

Funding

Research reported in this publication was supported by the National Institutes of Health (NIH) under Award Numbers R01EY019887 (DBG) and R01NS096173 (DBG), Research to Prevent Blindness (DBG), That Man May See (MM and DBG), and Knights Templar Eye Foundation (MM) and Bright Focus G20172018 (DBG), and in part by the UCSF Vision Core shared resource of the NIH/NEI P30 EY002162, and by an unrestricted grant from Research to Prevent Blindness, New York, NY. The content of this publication is solely the responsibility of the authors and does not necessarily represent the official views of the National Institutes of Health or other funding agencies.

Supplementary materials

Supplementary material associated with this article can be found, in the online version, at doi:10.1016/j.matbio.2022.05.001.

Received 21 December 2021;
Received in revised form 8 April 2022;
Accepted 2 May 2022
Available online 4 May 2022

Keywords:
Gould syndrome;
Anterior segment dysgenesis;
Basement membrane;
COL4A1;
COL4A2;
Type IV collagen;
TGFβ

Abbreviations:
ASD, anterior segment dysgenesis; CCT, central corneal thickness; OCT, optical coherence tomography; 4PBA, 4-phenylbutyrate

References

[1] D.B. Gould, S.W. John, Anterior segment dysgenesis and the developmental glaucomas are complex traits, Hum. Mol. Genet. 11 (10) (2002) 1185–1193.
[2] J.C. Sowden, Molecular and developmental mechanisms of anterior segment dysgenesis, Eye 21 (10) (2007) 1310–1318.
[3] L.M. Reis, E.V. Semina, Genetics of anterior segment dysgenesis disorders, Curr. Opin. Ophthalmol. 22 (5) (2011) 314–324.
[4] Y.A. Ito, M.A. Walter, Genomics and anterior segment dysgenesis: a review, Clin. Exp. Ophthalmol. 42 (1) (2014) 13–24.
[5] B. D'Haene, F. Meire, I. Claerhout, H.Y. Kroes, A. Plomp, Y.H. Arens, T. de Ravel, I. Casteels, S. De Jaegere, S. Hooghe, W. Wuyts, J. van den Ende, F. Roulez, H.E. Veenstra-Knol, R.A. Oldenburg, J. Giltay, J.B. Verheij, J.T. de Faber, B. Menten, A. De Paepe, P. Kestelyn, B.P. Leroy, E. De Baere, Expanding the spectrum of FOXC1 and PITX2 mutations and copy number changes in patients with anterior segment malformations, Investig. Ophthalmol. Vis. Sci. 52 (1) (2011) 324–333.
[6] A.S. Ma, J.R. Grigg, R.V. Jamieson, Phenotype-genotype correlations and emerging pathways in ocular anterior segment dysgenesis, Hum. Genet. 138 (8–9) (2019) 899–915.
[7] A. Ma, S. Yousoof, J.R. Grigg, M. Flaherty, A.E. Minoche, M.J. Cowley, B.M. Nash, G. Ho, T. Gayagay, T. Lai, E. Farnsworth, E.L. Hackett, K. Fisk, K. Wong, K.J. Holman, G. Jenkins, A. Cheng, F. Martin, T. Karaconji, J.E. Elder, A. Enriquez, M. Wilson, D.J. Amor, C.A. Stutterd, B. Kamien, J. Nelson, M.E. Dinger, B. Bennetts, R.V. Jamieson, Revealing hidden genetic diagnoses in the ocular anterior segment disorders, Genet. Med. 22 (10) (2020) 1623–1632.
[8] M.E. Meuwissen, D.J. Halley, L.S. Smit, M.H. Lequin, J.M. Cobben, R. de Coo, J. van Harssel, S. Sallevelt, G. Woldringh, M.S. van der Knaap, L.S. de Vries, G.M. Mancini, The expanding phenotype of COL4A1 and COL4A2 mutations: clinical data on 13 newly identified families and a review of the literature, Genet. Med. 17 (11) (2015) 843–853.
[9] M. Jeanne, D.B. Gould, Genotype-phenotype correlations in pathology caused by collagen type IV alpha 1 and 2 mutations, Matrix Biol. J. Int. Soc. Matrix Biol. 57-58 (2017) 29–44.
[10] M. Mao, T. Popli, M. Jeanne, K. Hoff, S. Sen, D.B. Gould, Identification of fibronectin 1 as a candidate genetic modifier in a *Col4a1* mutant mouse model of Gould syndrome, Dis. Model. Mech. 14 (4) (2021) dmm048231.
[11] I. Coupry, I. Sibon, B. Mortemousque, F. Rouanet, M. Mine, C. Goizet, Ophthalmological features associated with COL4A1 mutations, Arch. Ophthalmol. 128 (4) (2010) 483–489.
[12] S. Shah, S. Ellard, R. Kneen, M. Lim, N. Osborne, J. Rankin, N. Stoodley, M. van der Knaap, A. Whitney, P. Jardine, Childhood presentation of COL4A1 mutations, Dev. Med. Child Neurol. 54 (6) (2012) 569–574.
[13] E. Rodahl, P.M. Knappskog, J. Majewski, S. Johansson, W. Telstad, J. Krakenes, H. Boman, Variants of anterior segment dysgenesis and cerebral involvement in a large family with a novel COL4A1 mutation, Am. J. Ophthalmol. 155 (5) (2013) 946–953.
[14] S. Zagaglia, C. Selch, J.R. Nisevic, D. Mei, Z. Michalak, L. Hernandez-Hernandez, S. Krithika, K. Vezyroglou, S.M. Varadkar, A. Pepler, S. Biskup, M. Leao, J. Gartner, A. Merkenschlager, M. Jaksch, R.S. Moller, E. Gardella, B.S. Kristiansen, L.K. Hansen, M.S. Vari, K.L. Helbig, S. Desai, C.L. Smith-Hicks, N. Hino-Fukuyo, T. Talvik, R. Laugesaar, P. Ilves, K. Ounap, I. Korber, T. Hartlieb, M. Kudernatsch, P. Winkler, M. Schimmel, A. Hasse, M. Knuf, J. Heinemeyer, C. Makowski, S. Ghedia,

G.M. Subramanian, P. Striano, R.H. Thomas, C. Micallef, M. Thom, D.J. Werring, G.J. Kluger, J.H. Cross, R. Guerrini, S. Balestrini, S.M. Sisodiya, Neurologic phenotypes associated with COL4A1/2 mutations: expanding the spectrum of disease, Neurology 91 (22) (2018) e2078–e2088.

[15] A. Yaramis, H. Lochmuller, A. Topf, E. Sonmezler, E. Yilmaz, S. Hiz, U. Yis, S. Gungor, A. Ipek Polat, P. Edem, S. Beltran, S. Laurie, A. Yaramis, R. Horvath, Y. Oktay, COL4A1-related autosomal recessive encephalopathy in 2 Turkish children, Neurol. Genet. 6 (1) (2020) e392.

[16] S. Bakhtiari, A. Tafakhori, S.C. Jin, B.S. Guida, E. Alehabib, S. Firouzbadi, K. Bilguvar, M.C. Fahey, H. Darvish, M.C. Kruer, Recessive COL4A2 mutation leads to intellectual disability, epilepsy, and spastic cerebral palsy, Neurol. Genet. 7 (3) (2021) e583.

[17] D. Renard, M. Mine, E. Pipiras, P. Labauge, A. Delahaye, B. Benzacken, E. Tournier-Lasserve, Cerebral small-vessel disease associated with COL4A1 and COL4A2 gene duplications, Neurology 83 (11) (2014) 1029–1031.

[18] L. Kuuluvainen, S. Monkare, H. Kokkonen, F. Zhao, A. Verkkoniemi-Ahola, J. Schleutker, A.H. Hakonen, P. Hartikainen, M. Poyhonen, L. Myllykangas, COL4A1 and COL4A2 duplication causes cerebral small vessel disease with recurrent early onset ischemic strokes, Stroke 52 (10) (2021) e624–e625.

[19] S. Koene, C. Peeters-Scholte, J. Knijnenburg, L.S. de Vries, P.N.A. van Scheltema, M.E. Meuwissen, S.J. Steggerda, G.W.E. Santen, Intracerebral hemorrhage in a neonate with an intragenic COL4A2 duplication, Am. J. Med. Genet. A 185 (2) (2021) 571–574.

[20] K. Bilguvar, M.L. DiLuna, M.J. Bizzarro, Y. Bayri, K.C. Schneider, R.P. Lifton, M. Gunel, L.R. Ment, G Pacifier, Breastfeeding trial, COL4A1 mutation in preterm intraventricular hemorrhage, J. Pediatr. 155 (5) (2009) 743–745.

[21] M. Hausman-Kedem, L. Ben-Sira, D. Kidron, S. Ben-Shachar, R. Straussberg, D. Marom, P. Ponger, A. Bar-Shira, G. Malinger, A. Fattal-Valevski, Deletion in COL4A2 is associated with a three-generation variable phenotype: from fetal to adult manifestations, Eur. J. Hum. Genet. 29 (11) (2021) 1654–1662.

[22] A.H. Sabir, A. Singh, G. Elley, E. Wassemer, K. Foster, M. Sloman, D. Lim, A second report of recessive type COL4A1-related disorder: a novel homozygous missense variant, Clin. Dysmorphol. 30 (2) (2021) 115–119.

[23] E. Verdura, D. Herve, F. Bergametti, C. Jacquet, T. Morvan, C. Prieto-Morin, A. Mackowiak, E. Manchon, H. Hosseini, C. Cordonnier, I. Girard-Buttaz, S. Rosenstingl, C. Hagel, G. Kuhlenbaumer, E. Leca-Radu, D. Goux, L. Fleming, T. Van Agtmael, H. Chabriat, F. Chapon, E. Tournier-Lasserve, Disruption of a miR-29 binding site leading to COL4A1 upregulation causes pontine autosomal dominant microangiopathy with leukoencephalopathy, Ann. Neurol. 80 (5) (2016) 741–753.

[24] K. Rannikmae, D.E. Henshall, S. Thrippleton, Q. Ginj Kong, M. Chong, N. Grami, I. Kuan, T. Wilkinson, B. Wilson, K. Wilson, G. Pare, C. Sudlow, Beyond the brain: systematic review of extracerebral phenotypes associated with monogenic cerebral small vessel disease, Stroke 51 (10) (2020) 3007–3017.

[25] D.B. Gould, F.C. Phalan, G.J. Breedveld, S.E. van Mil, R.S. Smith, J.C. Schimenti, U. Aguglia, M.S. van der Knaap, P. Heutink, S.W. John, Mutations in *Col4a1* cause perinatal cerebral hemorrhage and porencephaly, Science 308 (5725) (2005) 1167–1171.

[26] T. Van Agtmael, U. Schlotzer-Schrehardt, L. McKie, D.G. Brownstein, A.W. Lee, S.H. Cross, Y. Sado, J.J. Mullins, E. Poschl, I.J. Jackson, Dominant mutations of *Col4a1* result in basement membrane defects which lead to anterior segment dysgenesis and glomerulopathy, Hum. Mol. Genet. 14 (21) (2005) 3161–3168.

[27] J. Favor, C.J. Gloeckner, D. Janik, M. Klempt, A. Neuhauser-Klaus, W. Pretsch, W. Schmahl, L. Quintanilla-Fend, Type IV procollagen missense mutations associated with defects of the eye, vascular stability, the brain, kidney function and embryonic or postnatal viability in the mouse, Mus musculus: an extension of the *Col4a1* allelic series and the identification of the first two *Col4a2* mutant alleles, Genetics 175 (2) (2007) 725–736.

[28] Z. Chen, T. Migeon, M.C. Verpont, M. Zaidan, Y. Sado, D. Kerjaschki, P. Ronco, E. Plaisier, HANAC syndrome *Col4a1* mutation causes neonate glomerular hyperpermeability and adult glomerulocystic kidney disease, J. Am. Soc. Nephrol. 27 (4) (2016) 1042–1054.

[29] C. Thaung, K. West, B.J. Clark, L. McKie, J.E. Morgan, K. Arnold, P.M. Nolan, J. Peters, A.J. Hunter, S.D. Brown, I.J. Jackson, S.H. Cross, Novel ENU-induced eye mutations in the mouse: models for human eye disease, Hum. Mol. Genet. 11 (7) (2002) 755–767.

[30] D.B. Gould, J.K. Marchant, O.V. Savinova, R.S. Smith, S.W. John, *Col4a1* mutation causes endoplasmic reticulum stress and genetically modifiable ocular dysgenesis, Hum. Mol. Genet. 16 (7) (2007) 798–807.

[31] C. Labelle-Dumais, D.J. Dilworth, E.P. Harrington, M. de Leau, D. Lyons, Z. Kabaeva, M.C. Manzini, W.B. Dobyns, C.A. Walsh, D.E. Michele, D.B. Gould, COL4A1 mutations cause ocular dysgenesis, neuronal localization defects, and myopathy in mice and Walker-Warburg syndrome in humans, PLos Genet. 7 (5) (2011) e1002062.

[32] M. Mao, R.S. Smith, M.V. Alavi, J.K. Marchant, M. Cosma, R.T. Libby, S.W. John, D.B. Gould, Strain-dependent anterior segment dysgenesis and progression to glaucoma in *Col4a1* mutant mice, Investig. Ophthalmol. Vis. Sci. 56 (11) (2015) 6823–6831.

[33] D.S. Kuo, C. Labelle-Dumais, M. Mao, M. Jeanne, W.B. Kauffman, J. Allen, J. Favor, D.B. Gould, Allelic heterogeneity contributes to variability in ocular dysgenesis, myopathy and brain malformations caused by *Col4a1* and *Col4a2* mutations, Hum. Mol. Genet. 23 (7) (2014) 1709–1722.

[34] M. Jeanne, J. Jorgensen, D.B. Gould, Molecular and genetic analyses of collagen type IV mutant mouse models of spontaneous intracerebral hemorrhage identify mechanisms for stroke prevention, Circulation 131 (18) (2015) 1555–1565.

[35] C. Labelle-Dumais, V. Schuitema, G. Hayashi, K. Hoff, W. Gong, D.Q. Dao, E.M. Ullian, P. Oishi, M. Margeta, D.B. Gould, COL4A1 mutations cause neuromuscular disease with tissue-specific mechanistic heterogeneity, Am. J. Hum. Genet. 104 (5) (2019) 847–860.

[36] X. Bai, D.J. Dilworth, Y.C. Weng, D.B. Gould, Developmental distribution of collagen IV isoforms and relevance to ocular diseases, Matrix Biol. J. Int. Soc. Matrix Biol. 28 (4) (2009) 194–201.

[37] K.J. Paavola, H. Sidik, J.B. Zuchero, M. Eckart, W.S. Talbot, Type IV collagen is an activating ligand for the

adhesion G protein-coupled receptor GPR126, Sci Signal 7 (338) (2014) ra76.
[38] J.D. Parkin, J.D. San Antonio, V. Pedchenko, B. Hudson, S.T. Jensen, J. Savige, Mapping structural landmarks, ligand binding sites, and missense mutations to the collagen IV heterotrimers predicts major functional domains, novel interactions, and variation in phenotypes in inherited diseases affecting basement membranes, Hum. Mutat. 32 (2) (2011) 127–143.
[39] M. Schroder, R.J. Kaufman, ER stress and the unfolded protein response, Mutat. Res. 569 (1–2) (2005) 29–63.
[40] V.M. Paralkar, S. Vukicevic, A.H. Reddi, Transforming growth factor beta type 1 binds to collagen IV of basement membrane matrix: implications for development, Dev. Biol. 143 (2) (1991) 303–308.
[41] X. Wang, R.E. Harris, L.J. Bayston, H.L. Ashe, Type IV collagens regulate BMP signalling in Drosophila, Nature 455 (7209) (2008) 72–77.
[42] V.M. Paralkar, B.S. Weeks, Y.M. Yu, H.K. Kleinman, A.H. Reddi, Recombinant human bone morphogenetic protein 2B stimulates PC12 cell differentiation: potentiation and binding to type IV collagen, J. Cell Biol. 119 (6) (1992) 1721–1728.
[43] S. Bunt, C. Hooley, N. Hu, C. Scahill, H. Weavers, H. Skaer, Hemocyte-secreted type IV collagen enhances BMP signaling to guide renal tubule morphogenesis in Drosophila, Dev. Cell 19 (2) (2010) 296–306.
[44] L.M. Ittner, H. Wurdak, K. Schwerdtfeger, T. Kunz, F. Ille, P. Leveen, T.A. Hjalt, U. Suter, S. Karlsson, F. Hafezi, W. Born, L. Sommer, Compound developmental eye disorders following inactivation of TGFbeta signaling in neural-crest stem cells, J. Biol. 4 (3) (2005) 11.
[45] S. Saika, S. Saika, C.Y. Liu, M. Azhar, L.P. Sanford, T. Doetschman, R.L. Gendron, C.W. Kao, W.W. Kao, TGFbeta2 in corneal morphogenesis during mouse embryonic development, Dev. Biol. 240 (2) (2001) 419–432.
[46] C. Flugel-Koch, A. Ohlmann, J. Piatigorsky, E.R. Tamm, Disruption of anterior segment development by TGF-beta1 overexpression in the eyes of transgenic mice, Dev. Dyn. 225 (2) (2002) 111–125 an official publication of the American Association of Anatomists.
[47] G. Proetzel, S.A. Pawlowski, M.V. Wiles, M. Yin, G.P. Boivin, P.N. Howles, J. Ding, M.W. Ferguson, T. Doetschman, Transforming growth factor-beta 3 is required for secondary palate fusion, Nat. Genet. 11 (4) (1995) 409–414.
[48] M.M. Shull, T. Doetschman, Transforming growth factor-beta 1 in reproduction and development, Mol. Reprod. Dev. 39 (2) (1994) 239–246.
[49] V. Kaartinen, J.W. Voncken, C. Shuler, D. Warburton, D. Bu, N. Heisterkamp, J. Groffen, Abnormal lung development and cleft palate in mice lacking TGF-beta 3 indicates defects of epithelial-mesenchymal interaction, Nat. Genet. 11 (4) (1995) 415–421.
[50] B. Chang, R.S. Smith, M. Peters, O.V. Savinova, N.L. Hawes, A. Zabaleta, S. Nusinowitz, J.E. Martin, M.L. Davisson, C.L. Cepko, B.L. Hogan, S.W. John, Haploinsufficient Bmp4 ocular phenotypes include anterior segment dysgenesis with elevated intraocular pressure, BMC Genet. 2 (2001) 18.
[51] A.J. Quantock, R.D. Young, Development of the corneal stroma, and the collagen-proteoglycan associations that help define its structure and function, Dev. Dyn. 237 (10) (2008) 2607–2621 an official publication of the American Association of Anatomists.
[52] P.Y. Lwigale, Corneal development: different cells from a common progenitor, Prog. Mol. Biol. Transl. Sci. 134 (2015) 43–59.
[53] J. Li, Y. Qin, F.K. Zhao, D. Wu, X.F. He, J. Liu, J.Y. Zhao, J.S. Zhang, Anterior segment dysgenesis correlation with epithelial-mesenchymal transition in Smad4 knockout mice, Int. J. Ophthalmol. 9 (7) (2016) 943–947.
[54] R. Zhang, H. Huang, P. Cao, Z. Wang, Y. Chen, Y. Pan, Sma- and Mad-related protein 7 (Smad7) is required for embryonic eye development in the mouse, J. Biol. Chem. 288 (15) (2013) 10275–10285.
[55] L.M. Reis, R.C. Tyler, K.F. Schilter, O. Abdul-Rahman, J.W. Innis, B.A. Kozel, A.S. Schneider, T.M. Bardakjian, E.J. Lose, D.M. Martin, U. Broeckel, E.V. Semina, BMP4 loss-of-function mutations in developmental eye disorders including SHORT syndrome, Hum. Genet. 130 (4) (2011) 495–504.
[56] A.W. Wyatt, R.J. Osborne, H. Stewart, N.K. Ragge, Bone morphogenetic protein 7 (BMP7) mutations are associated with variable ocular, brain, ear, palate, and skeletal anomalies, Hum. Mutat. 31 (7) (2010) 781–787.
[57] O. Puk, C. Dalke, J. Calzada-Wack, N. Ahmad, M. Klaften, S. Wagner, M.H. de Angelis, J. Graw, Reduced corneal thickness and enlarged anterior chamber in a novel Col-VIIIa2G257D mutant mouse, Investig. Ophthalmol. Vis. Sci. 50 (12) (2009) 5653–5661.
[58] C.Y. Liu, D.E. Birk, J.R. Hassell, B. Kane, W.W. Kao, Keratocan-deficient mice display alterations in corneal structure, J. Biol. Chem. 278 (24) (2003) 21672–21677.
[59] S. Chakravarti, W.M. Petroll, J.R. Hassell, J.V. Jester, J.H. Lass, J. Paul, D.E. Birk, Corneal opacity in lumican-null mice: defects in collagen fibril structure and packing in the posterior stroma, Investig. Ophthalmol. Vis. Sci. 41 (11) (2000) 3365–3373.
[60] P.J. Gage, W. Rhoades, S.K. Prucka, T. Hjalt, Fate maps of neural crest and mesoderm in the mammalian eye, Investig. Ophthalmol. Vis. Sci. 46 (11) (2005) 4200–4208.
[61] M.H. Strungaru, T. Footz, Y. Liu, F.B. Berry, P. Belleau, E.V. Semina, V. Raymond, M.A. Walter, PITX2 is involved in stress response in cultured human trabecular meshwork cells through regulation of SLC13A3, Investig. Ophthalmol. Vis. Sci. 52 (10) (2011) 7625–7633.
[62] M. Acharya, M.W. Sharp, F. Mirzayans, T. Footz, L. Huang, C. Birdi, M.A. Walter, Yeast two-hybrid analysis of a human trabecular meshwork cDNA library identified EFEMP2 as a novel PITX2 interacting protein, Mol. Vis. 18 (2012) 2182–2189.
[63] M. Acharya, D.J. Lingenfelter, L. Huang, P.J. Gage, M.A. Walter, Human PRKC apoptosis WT1 regulator is a novel PITX2-interacting protein that regulates PITX2 transcriptional activity in ocular cells, J. Biol. Chem. 284 (50) (2009) 34829–34838.
[64] A.H. Lin, J. Luo, L.H. Mondshein, P. ten Dijke, D. Vivien, C.H. Contag, T. Wyss-Coray, Global analysis of Smad2/3-dependent TGF-beta signaling in living mice reveals prominent tissue-specific responses to injury, J. Immunol. 175 (1) (2005) 547–554.
[65] Y. Shi, J. Massague, Mechanisms of TGF-beta signaling from cell membrane to the nucleus, Cell 113 (6) (2003) 685–700.
[66] Y. Tamimi, J.M. Skarie, T. Footz, F.B. Berry, B.A. Link, M.A. Walter, FGF19 is a target for FOXC1 regulation in

ciliary body-derived cells, Hum. Mol. Genet. 15 (21) (2006) 3229–3240.
[67] M. Inoue-Mochita, T. Inoue, T. Fujimoto, T. Kameda, N. Awai-Kasaoka, N. Ohtsu, K. Kimoto, H. Tanihara, p38 MAP kinase inhibitor suppresses transforming growth factor-beta2-induced type 1 collagen production in trabecular meshwork cells, PLoS One 10 (3) (2015) e0120774.
[68] M.H. Solheim, A.C. Clermont, J.N. Winnay, E. Hallstensen, A. Molven, P.R. Njolstad, E. Rodahl, C.R. Kahn, Iris malformation and anterior segment dysgenesis in mice and humans with a mutation in PI 3-kinase, Investig. Ophthalmol. Vis. Sci. 58 (7) (2017) 3100–3106.
[69] B. Rabiee, K.N. Anwar, X. Shen, I. Putra, M. Liu, R. Jung, N. Afsharkhamseh, M.I. Rosenblatt, G.A. Fishman, X. Liu, M. Ghassemi, A.R. Djalilian, Gene dosage manipulation alleviates manifestations of hereditary PAX6 haploinsufficiency in mice, Sci. Transl. Med. 12 (573) (2020) eaaz4894.
[70] F.A. Millan, F. Denhez, P. Kondaiah, R.J. Akhurst, Embryonic gene expression patterns of TGF beta 1, beta 2 and beta 3 suggest different developmental functions *in vivo*, Development 111 (1) (1991) 131–143.
[71] N. Dunker, K. Krieglstein, Reduced programmed cell death in the retina and defects in lens and cornea of Tgfbeta2(-/-) Tgfbeta3(-/-) double-deficient mice, Cell Tissue Res. 313 (1) (2003) 1–10.
[72] R. Blakytny, A. Ludlow, G.E. Martin, G. Ireland, L.R. Lund, M.W. Ferguson, G. Brunner, Latent TGF-beta1 activation by platelets, J. Cell. Physiol. 199 (1) (2004) 67–76.
[73] Y. Srinivasan, F.J. Lovicu, P.A. Overbeek, Lens-specific expression of transforming growth factor beta1 in transgenic mice causes anterior subcapsular cataracts, J. Clin. Investig. 101 (3) (1998) 625–634.
[74] M. Mao, M. Kiss, Y. Ou, D.B. Gould, Genetic dissection of anterior segment dysgenesis caused by a *Col4a1* mutation in mouse, Dis. Model. Mech. 10 (4) (2017) 475–485.
[75] A.B. Kulkarni, C.G. Huh, D. Becker, A. Geiser, M. Lyght, K.C. Flanders, A.B. Roberts, M.B. Sporn, J.M. Ward, S. Karlsson, Transforming growth factor beta 1 null mutation in mice causes excessive inflammatory response and early death, Proc. Natl. Acad. Sci. U. S. A. 90 (2) (1993) 770–774.
[76] L.P. Sanford, I. Ormsby, A.C. Gittenberger-de Groot, H. Sariola, R. Friedman, G.P. Boivin, E.L. Cardell, T. Doetschman, TGFbeta2 knockout mice have multiple developmental defects that are non-overlapping with other TGFbeta knockout phenotypes, Development 124 (13) (1997) 2659–2670.
[77] W. Heavner, L. Pevny, Eye development and retinogenesis, Cold Spring Harb. Perspect. Biol. 4 (12) (2012).
[78] D.C.H. van Dorst, N.P. de Wagenaar, I. van der Pluijm, J.W. Roos-Hesselink, J. Essers, A.H.J. Danser, Transforming growth factor-beta and the renin-angiotensin system in syndromic thoracic aortic aneurysms: implications for treatment, Cardiovasc. Drugs Ther. 35 (6) (2021) 1233–1252.
[79] G. Hayashi, C. Labelle-Dumais, D.B. Gould, Use of sodium 4-phenylbutyrate to define therapeutic parameters for reducing intracerebral hemorrhage and myopathy in *Col4a1* mutant mice, Dis. Model. Mech. 11 (7) (2018) dmm034157.
[80] M. Mao, M.V. Alavi, C. Labelle-Dumais, D.B. Gould, Type IV collagens and basement membrane diseases: cell biology and pathogenic mechanisms, Curr. Top. Membr. 76 (2015) 61–116.
[81] M.R. Silas, S.M. Hilkert, J.J. Reidy, A.V. Farooq, Posterior keratoconus, Br. J. Ophthalmol. 102 (7) (2018) 863–867.
[82] J. Swierkowska, M. Gajecka, Genetic factors influencing the reduction of central corneal thickness in disorders affecting the eye, Ophthalmic Genet. 38 (6) (2017) 501–510.
[83] E. Fransen, H. Valgaeren, K. Janssens, M. Sommen, R. De Ridder, G. Vandeweyer, L. Bisceglia, V. Soler, A. Hoischen, G. Mortier, F. Malecaze, C. Koppen, G. Van Camp, Resequencing of candidate genes for Keratoconus reveals a role for Ehlers-Danlos syndrome genes, Eur. J. Hum. Genet. 29 (12) (2021) 1745–1755.
[84] D.B. Gould, R.S. Smith, S.W. John, Anterior segment development relevant to glaucoma, Int. J. Dev. Biol. 48 (8–9) (2004) 1015–1029.
[85] C.R. French, S. Seshadri, A.L. Destefano, M. Fornage, C.R. Arnold, P.J. Gage, J.M. Skarie, W.B. Dobyns, K.J. Millen, T. Liu, W. Dietz, T. Kume, M. Hofker, D.J. Emery, S.J. Childs, A.J. Waskiewicz, O.J. Lehmann, Mutation of FOXC1 and PITX2 induces cerebral small-vessel disease, J. Clin. Investig. 124 (11) (2014) 4877–4881.
[86] T. Prasitsak, M. Nandar, S. Okuhara, S. Ichinose, M.S. Ota, S. Iseki, *Foxc1* is required for early stage telencephalic vascular development, Dev. Dyn. 244 (5) (2015) 703–711 an official publication of the American Association of Anatomists.
[87] T.R. Whitesell, P.W. Chrystal, J.R. Ryu, N. Munsie, A. Grosse, C.R. French, M.L. Workentine, R. Li, L.J. Zhu, A. Waskiewicz, O.J. Lehmann, N.D. Lawson, S.J. Childs, *foxc1* is required for embryonic head vascular smooth muscle differentiation in zebrafish, Dev. Biol. 453 (1) (2019) 34–47.
[88] F.E. Jones, L.S. Murray, S. McNeilly, A. Dean, A. Aman, Y. Lu, N. Nikolova, R. Malomgre, K. Horsburgh, W.M. Holmes, K.E. Kadler, T. Van Agtmael, 4-Sodium phenyl butyric acid has both efficacy and counter-indicative effects in the treatment of *Col4a1* disease, Hum. Mol. Genet. 28 (4) (2019) 628–638.
[89] H. Nakanishi, T. Sugiura, J.B. Streisand, S.M. Lonning, J.D. Roberts, TGF-beta-neutralizing antibodies improve pulmonary alveologenesis and vasculogenesis in the injured newborn lung, Am. J. Physiol. Lung Cell. Mol. Physiol. 293 (1) (2007) L151–L161.
[90] J.P. Habashi, D.P. Judge, T.M. Holm, R.D. Cohn, B.L. Loeys, T.K. Cooper, L. Myers, E.C. Klein, G. Liu, C. Calvi, M. Podowski, E.R. Neptune, M.K. Halushka, D. Bedja, K. Gabrielson, D.B. Rifkin, L. Carta, F. Ramirez, D.L. Huso, H.C. Dietz, Losartan, an AT1 antagonist, prevents aortic aneurysm in a mouse model of Marfan syndrome, Science 312 (5770) (2006) 117–121.
[91] E.R. Neptune, P.A. Frischmeyer, D.E. Arking, L. Myers, T.E. Bunton, B. Gayraud, F. Ramirez, L.Y. Sakai, H.C. Dietz, Dysregulation of TGF-beta activation contributes to pathogenesis in Marfan syndrome, Nat. Genet. 33 (3) (2003) 407–411.
[92] T.M. Holm, J.P. Habashi, J.J. Doyle, D. Bedja, Y. Chen, C. van Erp, M.E. Lindsay, D. Kim, F. Schoenhoff, R.D. Cohn, B.L. Loeys, C.J. Thomas, S. Patnaik, J.J. Marugan, D.P. Judge, H.C. Dietz, Noncanonical TGFbeta signaling contributes to aortic aneurysm progression in Marfan syndrome mice, Science 332 (6027) (2011) 358–361.
[93] J.P. Habashi, J.J. Doyle, T.M. Holm, H. Aziz, F. Schoenhoff, D. Bedja, Y. Chen, A.N. Modiri, D.P. Judge,

H.C. Dietz, Angiotensin II type 2 receptor signaling attenuates aortic aneurysm in mice through ERK antagonism, Science 332 (6027) (2011) 361–365.
[94] M.A. Hofmann Bowman, K.A. Eagle, D.M. Milewicz, Update on clinical trials of losartan with and without beta-blockers to block aneurysm growth in patients with Marfan syndrome: a review, JAMA Cardiol. 4 (7) (2019) 702–707.
[95] A. Pitcher, J. Emberson, R.V. Lacro, L.A. Sleeper, M. Stylianou, L. Mahony, G.D. Pearson, M. Groenink, B.J. Mulder, A.H. Zwinderman, J. De Backer, A.M. De Paepe, E. Arbustini, G. Erdem, X.Y. Jin, M.D. Flather, M.J. Mullen, A.H. Child, A. Forteza, A. Evangelista, H.H. Chiu, M.H. Wu, G. Sandor, A.B. Bhatt, M.A. Creager, R.B. Devereux, B. Loeys, J.C. Forfar, S. Neubauer, H. Watkins, C. Boileau, G. Jondeau, H.C. Dietz, C. Baigent, Design and rationale of a prospective, collaborative meta-analysis of all randomized controlled trials of angiotensin receptor antagonists in Marfan syndrome, based on individual patient data: a report from the Marfan treatment trialists' collaboration, Am. Heart J. 169 (5) (2015) 605–612.
[96] J.R. Cook, N.P. Clayton, L. Carta, J. Galatioto, E. Chiu, S. Smaldone, C.A. Nelson, S.H. Cheng, B.M. Wentworth, F. Ramirez, Dimorphic effects of transforming growth factor-beta signaling during aortic aneurysm progression in mice suggest a combinatorial therapy for Marfan syndrome, Arterioscler. Thromb. Vasc. Biol. 35 (4) (2015) 911–917.
[97] H.H. Yang, J.M. Kim, E. Chum, C. van Breemen, A.W. Chung, Effectiveness of combination of losartan potassium and doxycycline versus single-drug treatments in the secondary prevention of thoracic aortic aneurysm in Marfan syndrome, J. Thorac. Cardiovasc. Surg. 140 (2) (2010) 305−312 e2.
[98] J.J. Lee, J. Galatioto, S. Rao, F. Ramirez, K.D. Costa, Losartan attenuates degradation of aorta and lung tissue micromechanics in a mouse model of severe Marfan syndrome, Ann. Biomed. Eng. 44 (10) (2016) 2994–3006.
[99] H.H. Yang, J.M. Kim, E. Chum, C. van Breemen, A.W. Chung, Long-term effects of losartan on structure and function of the thoracic aorta in a mouse model of Marfan syndrome, Br. J. Pharmacol. 158 (6) (2009) 1503–1512.
[100] W. Xiong, T. Meisinger, R. Knispel, J.M. Worth, B.T. Baxter, MMP-2 regulates Erk1/2 phosphorylation and aortic dilatation in Marfan syndrome, Circ. Res. 110 (12) (2012) e92–e101.
[101] D.A. Sica, T.W. Gehr, S. Ghosh, Clinical pharmacokinetics of losartan, Clin. Pharmacokinet. 44 (8) (2005) 797–814.
[102] S. Eguchi, T. Kawai, R. Scalia, V. Rizzo, Understanding angiotensin II type 1 receptor signaling in vascular pathophysiology, Hypertension 71 (5) (2018) 804–810.
[103] A.D. Bradshaw, K.M. McNagny, D.B. Gervin, G.M. Cann, T. Graf, D.O. Clegg, Integrin alpha 2 beta 1 mediates interactions between developing embryonic retinal cells and collagen, Development 121 (11) (1995) 3593–3602.
[104] P.J. Lein, D. Higgins, D.C. Turner, L.A. Flier, V.P. Terranova, The NC1 domain of type IV collagen promotes axonal growth in sympathetic neurons through interaction with the alpha 1 beta 1 integrin, J. Cell Biol. 113 (2) (1991) 417–428.
[105] K. Venstrom, L. Reichardt, Beta 8 integrins mediate interactions of chick sensory neurons with laminin-1, collagen IV, and fibronectin, Mol. Biol. Cell 6 (4) (1995) 419–431.
[106] X. Chen, H. Wang, H.J. Liao, W. Hu, L. Gewin, G. Mernaugh, S. Zhang, Z.Y. Zhang, L. Vega-Montoto, R.M. Vanacore, R. Fassler, R. Zent, A. Pozzi, Integrin-mediated type II TGF-beta receptor tyrosine dephosphorylation controls SMAD-dependent profibrotic signaling, J. Clin. Investig. 124 (8) (2014) 3295–3310.
[107] K. Iwao, M. Inatani, Y. Matsumoto, M. Ogata-Iwao, Y. Takihara, F. Irie, Y. Yamaguchi, S. Okinami, H. Tanihara, Heparan sulfate deficiency leads to Peters anomaly in mice by disturbing neural crest TGF-beta2 signaling, J. Clin. Investig. 119 (7) (2009) 1997–2008.
[108] M.A. Stepp, Corneal integrins and their functions, Exp. Eye Res. 83 (1) (2006) 3–15.
[109] S.K. Parapuram, K. Huh, S. Liu, A. Leask, Integrin beta1 is necessary for the maintenance of corneal structural integrity, Investig. Ophthalmol. Vis. Sci. 52 (11) (2011) 7799–7806.
[110] M.S. Filla, J.A. Faralli, J.L. Peotter, D.M. Peters, The role of integrins in glaucoma, Exp. Eye Res. 158 (2017) 124–136.
[111] M. Pathania, Y. Wang, V.N. Simirskii, M.K. Duncan, Beta1-integrin controls cell fate specification in early lens development, Differentiation 92 (4) (2016) 133–147.
[112] K.M. Tharp, R. Higuchi-Sanabria, G.A. Timblin, B. Ford, C. Garzon-Coral, C. Schneider, J.M. Muncie, C. Stashko, J.R. Daniele, A.S. Moore, P.A. Frankino, S. Homentcovschi, S.S. Manoli, H. Shao, A.L. Richards, K.H. Chen, J.T. Hoeve, G.M. Ku, M. Hellerstein, D.K. Nomura, K. Saijo, J. Gestwicki, A.R. Dunn, N.J. Krogan, D.L. Swaney, A. Dillin, V.M. Weaver, Adhesion-mediated mechanosignaling forces mitohormesis, Cell Metab. 33 (7) (2021) 1322−1341 e13.
[113] K.R. Monk, K. Oshima, S. Jors, S. Heller, W.S. Talbot, Gpr126 is essential for peripheral nerve development and myelination in mammals, Development 138 (13) (2011) 2673–2680.
[114] K.R. Monk, S.G. Naylor, T.D. Glenn, S. Mercurio, J.R. Perlin, C. Dominguez, C.B. Moens, W.S. Talbot, A G protein-coupled receptor is essential for Schwann cells to initiate myelination, Science 325 (5946) (2009) 1402–1405.
[115] M. Yebra, A.M. Montgomery, G.R. Diaferia, T. Kaido, S. Silletti, B. Perez, M.L. Just, S. Hildbrand, R. Hurford, E. Florkiewicz, M. Tessier-Lavigne, V. Cirulli, Recognition of the neural chemoattractant Netrin-1 by integrins alpha6-beta4 and alpha3beta1 regulates epithelial cell adhesion and migration, Dev. Cell 5 (5) (2003) 695–707.
[116] T. Xiao, W. Staub, E. Robles, N.J. Gosse, G.J. Cole, H. Baier, Assembly of lamina-specific neuronal connections by slit bound to type IV collagen, Cell 146 (1) (2011) 164–176.
[117] E. Poschl, U. Schlotzer-Schrehardt, B. Brachvogel, K. Saito, Y. Ninomiya, U. Mayer, Collagen IV is essential for basement membrane stability but dispensable for initiation of its assembly during early development, Development 131 (7) (2004) 1619–1628.
[118] C.D. Bryan, M.A. Casey, R.L. Pfeiffer, B.W. Jones, K.M. Kwan, Optic cup morphogenesis requires neural crest-mediated basement membrane assembly, Development 147 (4) (2020) dev181420.
[119] M. Takeuchi, S. Yamaguchi, S. Yonemura, K. Kakiguchi, Y. Sato, T. Higashiyama, T. Shimizu, M. Hibi, Type IV collagen controls the axogenesis of cerebellar granule cells by regulating basement membrane integrity in zebrafish, PLos Genet. 11 (10) (2015) e1005587.
[120] I. Sibon, I. Coupry, P. Menegon, J.P. Bouchet, P. Gorry, I. Burgelin, P. Calvas, I. Orignac, V. Dousset, D. Lacombe, J.M. Orgogozo, B. Arveiler, C. Goizet, COL4A1 mutation in

Axenfeld-Rieger anomaly with leukoencephalopathy and stroke, Ann. Neurol. 62 (2) (2007) 177–184.
[121] B. Deml, L.M. Reis, M. Maheshwari, C. Griffis, D. Bick, E.V. Semina, Whole exome analysis identifies dominant COL4A1 mutations in patients with complex ocular phenotypes involving microphthalmia, Clin. Genet. 86 (5) (2014) 475–481.
[122] E. Giorgio, G. Vaula, G. Bosco, S. Giacone, C. Mancini, A. Calcia, S. Cavalieri, E. Di Gregorio, R. Rigault De Longrais, S. Leombruni, L. Pinessi, P. Cerrato, A. Brusco, A. Brussino, Two families with novel missense mutations in COL4A1: when diagnosis can be missed, J. Neurol. Sci. 352 (1−2) (2015) 99–104.
[123] J.M. Plancher, R.B. Hufnagel, A. Vagal, K. Peariso, H.M. Saal, J.P. Broderick, Case of small vessel disease associated with COL4A1 mutations following trauma, Case Rep. Neurol. 7 (2) (2015) 142–147.
[124] D. Matias-Perez, L.A. Garcia-Montano, M. Cruz-Aguilar, I.A. Garcia-Montalvo, J. Nava-Valdez, T. Barragan-Arevalo, C. Villanueva-Mendoza, C.E. Villarroel, C. Guadarrama-Vallejo, R.V. la Cruz, O. Chacon-Camacho, J.C. Zenteno, Identification of novel pathogenic variants and novel gene-phenotype correlations in Mexican subjects with microphthalmia and/or anophthalmia by next-generation sequencing, J. Hum. Genet. 63 (11) (2018) 1169–1180.
[125] S. Nau, E.A. McCourt, J.A. Maloney, J.L. Van Hove, M. Saenz, J.L. Jung, COL4A1 mutations in two infants with congenital cataracts and porencephaly: an ophthalmologic perspective, J. AAPOS 23 (4) (2019) 246–248.
[126] R.C. Tripathi, J. Li, W.F. Chan, B.J. Tripathi, Aqueous humor in glaucomatous eyes contains an increased level of TGF-beta 2, Exp. Eye Res. 59 (6) (1994) 723–727.
[127] G. Picht, U. Welge-Luessen, F. Grehn, E. Lutjen-Drecoll, Transforming growth factor beta 2 levels in the aqueous humor in different types of glaucoma and the relation to filtering bleb development, Graefes Arch. Clin. Exp. Ophthalmol. 239 (3) (2001) 199–207.
[128] R. Fuchshofer, The pathogenic role of transforming growth factor-beta2 in glaucomatous damage to the optic nerve head, Exp. Eye Res. 93 (2) (2011) 165–169.
[129] M.A. Prendes, A. Harris, B.M. Wirostko, A.L. Gerber, B. Siesky, The role of transforming growth factor beta in glaucoma and the therapeutic implications, Br. J. Ophthalmol. 97 (6) (2013) 680–686.
[130] R. Fuchshofer, E.R. Tamm, The role of TGF-beta in the pathogenesis of primary open-angle glaucoma, Cell Tissue Res. 347 (1) (2012) 279–290.
[131] X.M. Meng, P.M. Tang, J. Li, H.Y. Lan, TGF-beta/Smad signaling in renal fibrosis, Front. Physiol. 6 (2015) 82.
[132] P. ten Dijke, H.M. Arthur, Extracellular control of TGFbeta signalling in vascular development and disease, Nat. Rev. Mol. Cell Biol. 8 (11) (2007) 857–869.
[133] M.J. Williams, T. Sugatani, O.A. Agapova, Y. Fang, J.P. Gaut, M.C. Faugere, H.H. Malluche, K.A. Hruska, The activin receptor is stimulated in the skeleton, vasculature, heart, and kidney during chronic kidney disease, Kidney Int. 93 (1) (2018) 147–158.
[134] S. Paylakhi, C. Labelle-Dumais, N.G. Tolman, M.A. Sellarole, Y. Seymens, J. Saunders, H. Lakosha, W.N. deVries, A.C. Orr, P. Topilko, S.W. John, K.S. Nair, Muller glia-derived PRSS56 is required to sustain ocular axial growth and prevent refractive error, PLos Genet. 14 (3) (2018) e1007244.
[135] K.J. Livak, T.D. Schmittgen, Analysis of relative gene expression data using real-time quantitative PCR and the 2 (-Delta Delta C(T)) Method, Methods 25 (4) (2001) 402–408.
[136] G. Yu, L.G. Wang, Y. Han, Q.Y. He, clusterProfiler: an R package for comparing biological themes among gene clusters, OMICS 16 (5) (2012) 284–287.
[137] Y. Liao, J. Wang, E.J. Jaehnig, Z. Shi, B. Zhang, WebGestalt 2019: gene set analysis toolkit with revamped UIs and APIs, Nucleic Acids Res. 47 (W1) (2019) W199–W205.
[138] B. Zhang, S. Kirov, J. Snoddy, WebGestalt: an integrated system for exploring gene sets in various biological contexts, Nucleic Acids Res. 33 (Web Server issue) (2005) W741–W748.
[139] M. Martens, A. Ammar, A. Riutta, A. Waagmeester, D.N. Slenter, K. Hanspers, A.M. R, D. Digles, E.N. Lopes, F. Ehrhart, L.J. Dupuis, L.A. Winckers, S.L. Coort, E.L. Willighagen, C.T. Evelo, A.R. Pico, M. Kutmon, WikiPathways: connecting communities, Nucleic Acids Res. 49 (D1) (2021) D613–D621.
[140] A.R. Pico, T. Kelder, M.P. van Iersel, K. Hanspers, B.R. Conklin, C. Evelo, WikiPathways: pathway editing for the people, PLoS Biol. 6 (7) (2008) e184.
[141] Z. He, F. Forest, P. Gain, D. Rageade, A. Bernard, S. Acquart, M. Peoc'h, D.M. Defoe, G. Thuret, 3D map of the human corneal endothelial cell, Sci. Rep. 6 (2016) 29047.